TALLINN UNIVERSITY OF TECHNOLOGY

FACAULT OF CHEMICAL AND MATERIALS TECHNOLOGY
DEPARTMENT OF MATERIAL SCIENCE
CHAIR OF SEMICONDUCTOR MATERIAL TECHNOLOGY

Optimization of Buffer Layer for Copper-Zinc-Tin-Sulfide-based Solar Cells

Master Thesis

Sha Li

Supervisor: Senior Research Scientist Mare Altosaar,
Chair of Semiconductor Materials Technology

Co-supervisor: Research Scientist Maris Pilvet,
Chair of Semiconductor Materials Technology

Materials and Processes of Sustainable Energetics
Tallinn 2016

Declaration

Hereby I declare that this master thesis, my original investigation and achievement, submitted for the master degree at Tallinn University of Technology has not been submitted for any degree or examination.

.....Sha Li.....
(Author's signature)

TALLINNA TEHNIKAÜLIKOOL

KEEMIA- JA MATERJALITEHNOLOOGIA TEADUSKOND

MATERJALITEADUSE INSTITUUT

POOLJUHTMATERJALIDE TEHNOLOOGIA ÕPPETOOL

Vask-tsink-tina-sulfiid-tüüpi Päikesepatarei Puhverkihi Optimiseerimine

Magistritöö

Sha Li

Juhendaja: Mare Altosaar, vanemteadur

Pooljuhtmaterjalide tehnoloogia õppetool

Kaasjuhendaja: Maris Pilvet, teadur

Pooljuhtmaterjalide tehnoloogia õppetool

Materjalid ja protsessid jätkusuutlikkus energeetikas

Tallinna 2016

MASTER THESIS ASSIGNMENT PLAN

Student data:

Name of the student: Sha Li Student Code: 145142KAYM

Master' s thesis topic:

"Optimization of Buffer Layer for Copper-Zinc-Tin-Sulfide-based Solar Cells" (in English)

"Vask-tsink-tina-sulfiid-tüüpi päikesepatarei puhverkihi optimiseerimine" (in Estonian)

Supervisor:

Name: Mare Altosaar, senior research scientist
Employment: Tallinn University of Technology, Faculty of Chemical and Materials Technology, Department of Material Science, Chair of Semiconductor Materials Technology
Profession: Senior Research Scientist

Co-supervisor:

Name: Maris Pilvet, research scientist
Employment: Tallinn University of Technology, Faculty of Chemical and Materials Technology, Department of Material Science, Chair of Semiconductor Materials Technology
Profession: Research Scientist

Aim and task of master's thesis:

To optimize buffer layer for copper-zinc-sulfide-based solar cells and improve copper-zinc-sulfide-based solar cells' performance

TABLE OF CONTENTS

List of Abbreviations and symbols

CZTS-Cu_2ZnSnS_4

CZTSSe- $Cu_2ZnSn(SSe)_4$

CIS –$CuInSe_2$ - copper indium selenide

CIGS-$Cu(InGa)Se_2$ - copper indium-gallium selenide

CIGSSe-$Cu(InGa)(SSe)_2$ - copper indium-gallium sulphoselenide

CBD-Chemical bath deposition

CBO-Conduction band offset

Eg-Band gap

FF-Fill factor

I-V-Current-voltage

J_{sc}-Short circuit current density

V_{oc}-Open circuit voltage

η-Solar cell efficiency

KCN-Potassium cyanide

MGL solar cell-Monograin layer solar cell

PV- Photovoltaic

SEM-Scanning electron microscopy

EDX-Energy-dispersive X-ray spectroscopy

PL-Photoluminescence

TWP-Terawatt power

GWp/y-Gigawatt power/year

TU-Thiourea

TAA-Thioacetamide

ΔE_c -Conduction band offset

ΔE_v- Valence band offset

PVD- Physical vapour deposition

ALD- Atomic layer deposition

MOCVD- Metal-organic chemical vapour deposition

ILGAR -Ion layer gas reaction deposition

ITO-Indium tin oxide

1. INTRODUCTION

Since the large increased consumption of fossil fuels and its consequence of environmental crisis have already attracted a great attention in the research and application of solar cells. Among of them, thin film solar cell development and commercialization has been growing fast in the past decade, because of their low cost and scalability. Due to the lower demand of materials, the thin-film solar cell technology can effectively reduce the cost of materials. In addition, thin film materials can be technically deposited on different substrates, such as glass, stainless steel and flexible polymer layers. This may lead to solar-powered building work. There is a huge demand for photovoltaic operations in 2020-2040 [1]. The demand for photovoltaic power generation will increase 20-150 GWp/y. This will include about 30% of the market taken by the thin films. Thin film solar cells are based mainly on CdTe, amorphous silicon, CIS, CIGS, CIGSSe, GaAs, and Cu_2ZnSnS_4 (CZTS). Among them, GaAs and CdTe have toxic elements (Cd, Te, As) and CIS-based cells contain rare elements indium and gallium [2]. Therefore, large area solar cell TWP applications can't be based on these two types of solar cell absorbers in the future [3]. The CZTS is I_2-II-IV-VI_4 group quaternary compound with kesterite structure. Its band gap is about 1.5eV which is optimum energy band gap for solar energy conversion. This band gap value is very close to the theoretical Shockley-Queisser limit of the single *p-n* junction semiconductor solar cell (1.35 eV) [4]. CZTS is a direct band gap semiconductor material having a high absorption coefficient [5]. Therefore, it can be used as an absorption layer in thin film solar cells. Currently commercialized crystalline silicon, CdTe and CIGS are lacking in earth abundance, non-toxic nature and environmentally friendliness. Compared to these above said qualities CZTS is the best candidate for thin film absorber material for the next generation thin film solar cells. Recently, it has been announced that CZTS-type thin film solar cells have already reached more than 12.6% efficiency based on its associated sulfo-selenide (CZTSSe) material [6]. This efficiency is already close to the commercialized CIGS efficiency. Though CZTS is considered as a potential substitute for the CIGSSe as absorber material, the formation of *p-n* junction with proper electronic characteristics is very important to achieve for a good device performance, in particular the band alignment between the CdS (*n-type*) and CZTS (*p-type*) materials. Therefore in the present thesis deposition of CdS is modified by using different Cd-salts as precursors and by applying hybrid buffer layer by sequential deposition of CdS and In_2S_3 layers.

The focus of this work is to modify 1) the Cd^{2+} ion source for CdS deposition with the aim to find the optimal Cd^{2+} reagent for the recepy used so far for CZTS monograin layer (MGL) solar cells; and 2) the deposition time to find the optimum time for CdS deposition. Due to the non-ideal band alignment at the CdS/CZTS interface, particularly the conduction band alignment plays a crucial role for the electron transport towards the front contact [7]. We studied also the effect of In_2S_3/CdS hybrid buffer layer to the CZTS MGL solar cells performance.

2. LITERATURE REVIEW AND THE OBJECTIVE OF STUDY

2.1. Photovoltaic solar cell

A solar cell or photovoltaic cell is an electrical device that converts the energy of light directly into electricity by photovoltaic effect, which is a physical and chemical phenomenon. Light, shining on the solar cell, produces both, a current and a voltage to generate electric power. A variety of materials and processes can potentially satisfy the requirements for photovoltaic energy conversion, but in practice nearly all photovoltaic energy conversion devices use semiconductor materials in the form of a *p-n junction*. [8]

2.1.1. *p-n* junction

A solar cell is a diode made of a *p-type* semiconductor and *n-type* semiconductor. In *p-type* semiconductor, holes are the majority carriers and electrons are the minority carriers, in *n-type* semiconductor electrons are the majority carriers and holes are the minority carriers. When two type semiconductor materials, *p-type* and *n-type* are brought to contact, majority carriers of each type would diffuse across the junction. This means that the majority carriers - holes from *p-type* diffuse to *n-type* material and the majority carriers of *n-type* diffuse to *p-type* material. The diffusion would stop after an electric field is built up sufficiently high to oppose diffusion. As the majority carrier such as hole diffuses across the junction, it combines with electron in the *n-type* side, creating a net positive charge. Likewise, the majority carrier electron from *n-type* material diffuses across the junction, recombines with hole in *p-type* side and creates net negative charge. The net charge at each side creates an electric field in the direction, which would oppose further diffusion. The electric field created would drift the minority carrier in the opposite direction across the junction. Thus when equilibrium attained, the drift carriers and diffused carriers should be balanced in termed of magnitude and in opposite direction. Mathematically, current density J due to various carrier types can be written as shown in equation (1) and (2).

$$J_p\,(\text{drift}) + J_p\,(\text{diff.}) = 0 \qquad (1)$$

$$J_n\,(\text{drift}) + J_n\,(\text{diff.}) = 0 \qquad (2)$$

As the result of this process, a depletion region - meaning a region that lack of carrier of certain thickness - is created at both side of the junction. At times, the depletion region is also termed as space charge region. The flow process of carriers in *p-type* and *n-type* materials is illustrated in Figure 1 to Figure 3, aslo the process how equilibrium is attained when *p-type* and *n-type* materials are contacted [9].

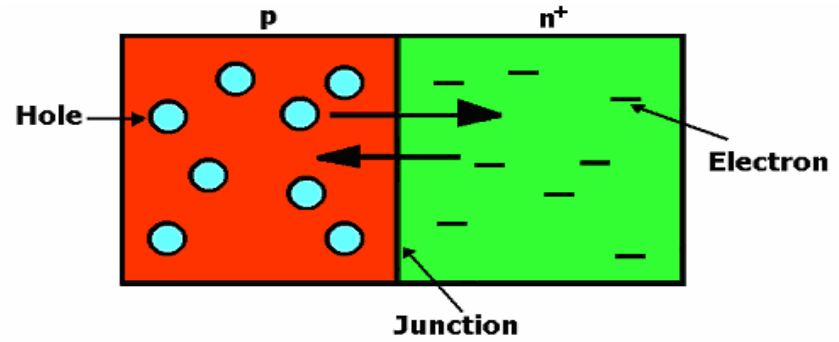

Figure 1. Majority carrier diffusion in *p-n* junction [9].

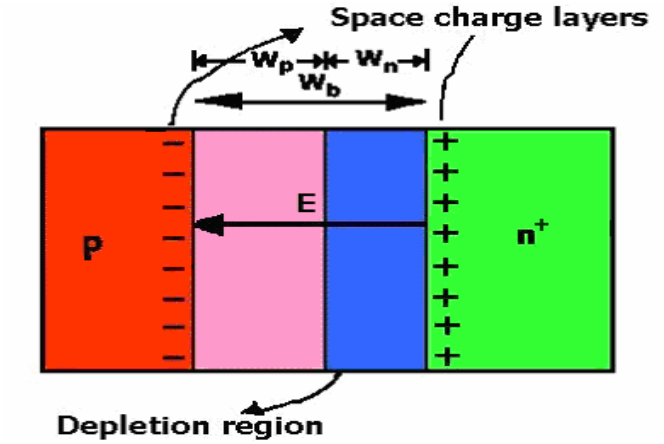

Figure 2. Depletion region, space charge layer and electric field forming in a *p-n* junction [9].

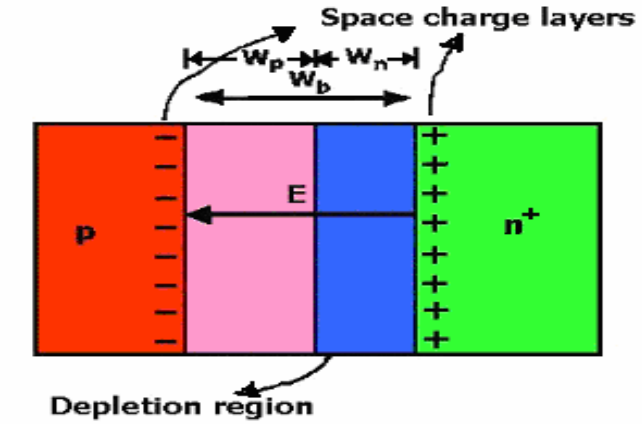

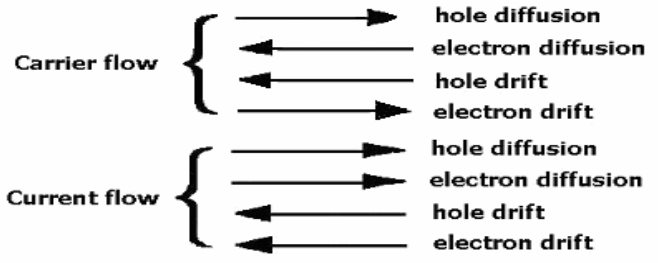

Figure 3. The carrier current at equilibrium cross a *p-n* junction [9].

2.1.2. Photovoltaic effect

When the *p-n* diode is exposed to light, the photon whose energy is larger than band gap value of semiconductor will excite an electron from the valence band to the conduction band leaving a hole in the valence band to produce an electron-hole pairs. Electrons can drift to *n*-region under the influence of built-in electric field and holes can easily drift to *p*-region under the influence of the built-in electric field, so this drift current generates the electric current. If the *p-n* junction is connected to external load, it will produce the electric current in the external circuit to complete whole process of conversion of light into electricity [10].

Due to the holes as the majority carriers in *p-type* semiconductor, number of free electrons in the conduction band is less, therefore the Fermi level is close to the valence band. The free electrons in *n-type* semiconductor are the majority carriers and the Fermi level is close to the conduction band. When the *n-type* semiconductor meets the *p-type* semiconductor, the Fermi level in the equilibrium state is consistent. When there is light, the electrons in the valence band will be excited to conduction band, and left a hole in the valance band. Electrons start to move towards the low energy terminal, and holes start to move towards the high energy terminal, thus the electric current is generated [11].

2.2. Structure of monograin layer (MGL) solar cells

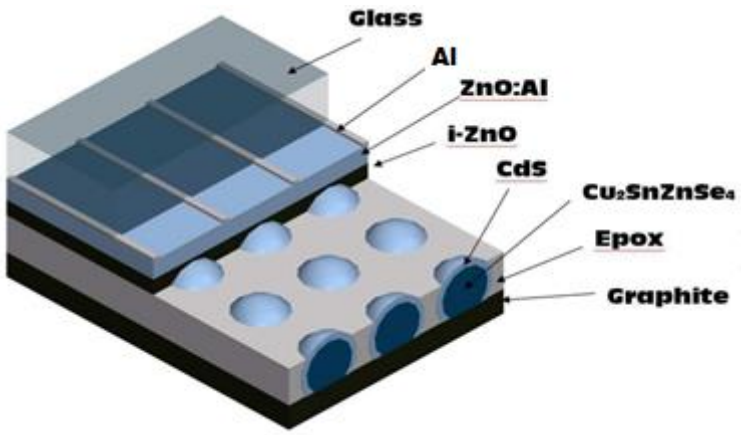

Figure 4. The device structure of MGL solar cell: graphite back contact/CZT(S)Se absorber/CdS buffer/i-ZnO/ZnO:Al window layer/ glass (or flexible) substrate [12].

Monograin is a single-crystalline powder particle consisting of one single crystal or several single-crystalline blocks grown into a compact grain [13]. The monograin layer (MGL) solar cells have a superstrate structure of graphite/MGL/CdS/ZnO/glass, where the MGL is a monolayer of powder grains of one size embedded into an organic resin (epoxy) so that the upper part of the grains remains uncovered. CdS is deposited on top of the MGL (or onto the surface of the monograins berfore MGL formation) by chemical bath deposition, followed by RF-sputtering of i-ZnO and conductive ZnO:Al layers. Finally, highly conductive grid contacts are evaporated on top of the ZnO window layer, and the structure is glued onto a glass or some other durable transparent substrate. For back contacting, the opening of back contact areas of the crystals that are originally inside the epoxy is done by etching the epoxy in H_2SO_4 for several seconds, followed by abrasive treatment. Subsequently, graphite paste for the back contact. The MGLs combine the advantages of polycrystalline materials and technologies and the high photoelectrical parameters of single crystals, that is, simple technology and low cost of materials and devices. MGL technology allows the separation of materials formation from module fabrication. Large area modules are fabricated at room temperature in a continuous roll-to-roll process. Homogeneous composition of powders gives an additional advantage, leading to homogeneous modules without any up-scaling problem [14].

2.3. Properties of CZTS absorber materials

Cu_2ZnSnS_4 is a quaternary compound semiconductor that crystallizes in thermodynamically stable body-centred tetragonal kesterite structure (Space group I_4) [15]. Cu_2ZnSnS_4 is one of the I_2-II-IV-VI_4 group materials that can be derived from $CuInS_2$ by substituting In (III) with Zn (II) and Sn (IV). The reported lattice constants of kesterite CZTS are as follows: a ≈ 5.419 Å, b ≈ 10.854 Å and c/2a ≈ 1.0015 Å and the band gap value is 1.5 eV [16]. The band gap value can be altered from 1.5 eV to 1 eV by substituting S by Se [14]. The single phase composition region is much narrower for CZTS than for CIGS. A very high absorption coefficient in the visible wavelength region makes this quaternary semiconductor favorable for PV device. In 2012, IBM developed an 11.1% efficient CZTS solar cell [17]. CZTS thin film absorber material can be prepared by vacuum and non vacuum based methods. The vacuum based methods are mainly adopted for controlling deposition parameters in order to obtain desired stoichiometric ratio and crystalline quality. Non-vacuum methods are mainly adopted for reducing material cost and simplified method for production. However, the unlike to CIGS films, non-vacuum methods were shown as high efficiencies for CZTS solar cells. Controlling the binaries during large area deposition is very difficult in non-vacuum process [18]. There are wide varieties of non-vacuum methods available for preparing CZTS thin films.

2.4. The role of buffer layer in *p-n* junction solar cell, buffer layer materials

The main role of a buffer layer in a heterojunction is to form a junction with the absorber layer while admitting a maximum amount of light to the junction region and absorber layer [19]. In addition, this layer should have minimal absorption losses and should be capable of driving out the photo-generated carries with minimum recombination losses and transporting the photo generated carriers to the outer circuit with minimal electrical resistance. For high optical throughput with minimal resistive loss the band gap of the buffer layer should be as high as possible and the layer should be as thin as possible to maintain low series resistance. It is also important that any potential ‘spike’ in the conduction band at the heterojunction has to be minimized for optimal minority carrier transport. Lattice mismatch (and consequent effects) at the junction is important for consideration for epitaxial or highly oriented layers.

2.4.1. Requirements for buffer layer materials in the CZTS-based solar cells

Here are the requirements for buffer materials listed below.

(1) The material should be *n-type* in order to form a *p-n* junction with the absorber layer.
(2) Large energy band gap for high optical transmission in the visible region.
(3) It has to be a stable compound.
(4) Optimal band discontinuities: Ideal solar cell junction will separate electrons and holes, letting through only one carrier type. This may be achieved if the energy band discontinuity, between the wide band gap buffer layer and the absorber material, is distributed in such a way that there is no band offset for the minority carriers. However, there should be a large barrier for majority carrier. The second condition is fulfilled if the first is fulfilled, provided the difference between the band gaps is significant. If there is a band offset for the minority carriers in the buffer layer, then it may lead to the formation of 'spike' or a 'cliff', depending on sign of the offset. If the band offset produces a cliff, probability of the interface cross-recombination is increased, and flat band condition is achieved at bias smaller than E_g/q of the absorber [20]. One consequence is that output voltage of the cell is limited in this case, because of the lack of barrier height. Band alignment with a moderate spike is rather optimal, although the presence of a spike means the band offset for the minority carrier decreases and the interface becomes less selective. In a more general case even a moderate spike may be dangerous as far as efficiency is concerned. Band discontinuities are usually studied using photoemission spectroscopy. [21, 22]
(5) Lattice mismatch (and consequent effects) at the junction is important for consideration for epitaxial or highly oriented layers.
(6) The process for deposition should be low cost and suitable for wide area deposition. In addition the technique should have capability to passivate the surface states of the absorber layer.

2.4.2. CdS buffer material

CdS is an *n-type* semiconductor with wide band gap (2.4 eV at room temperature). It posses good optical transmittance and electrical properties that make it as one of the ideal materials for their application to solar cell fabrication. CdS is one of the important materials for

application in electro-optic devices such as photo conducting cells, photosensors, transducers, laser materials, optical wave-guides and non-linear integrated optical devices, also used as photo catalyst [23-26]. The thickness of CdS should be less than 100 nm to avoid high value of series resistance and increase transmission of the layer.

2.4.3. In_2S_3 buffer material

Indium sulfide (In_2S_3) is a semiconducting compound belonging to III-VI family [27] Indium sulphide has strong anisotropic features in its crystal structure and crystallizes in three crystallographic configurations, namely, α, β and γ- In_2S_3. The most stable one is β- In_2S_3 which has a tetragonal structure [28]. For single crystal the direct optical band gap varies 2.0-2.45 eV [29], depending on composition. Being a wide band gap semiconductor, thin films of In_2S_3 are investigated for optoelectronics and photovoltaic applications. In recent years, In_2S_3 has been proved to be a promising buffer layer in the fabrication of $Cu(In,Ga)Se_2$ thin film solar cells due to its low toxicity compared to CdS [30].

2.4.4. The growth methods of buffer materials

The deposition methods used were: electrodeposition, chemical bath deposition (CBD), physical vapour deposition (PVD), atomic layer deposition (ALD), spray pyrolysis, metal-organic chemical vapour deposition (MOCVD), sputtering, ion layer gas reaction (ILGAR) and vacuum evaporation. Among these deposition processes, CBD is applied intensively for deposition of buffer layers on different substrates due to its low cost and simplicity and largely used method to prepare reproducible and homogeneous films at low temperatures [31].

CBD is applied intensively for deposition of buffer layers on different substrates due to its low cost and simplicity. In this thesis the chemical bath deposition process is used to deposit CdS and In_2S_3 as the buffer layer in monograin layer solar cells.

2.5. Chemical bath deposition

Chemical bath deposition (CBD) is the analog in liquid phase of the well-known chemical vapor deposition technique in the vapor phase. In CBD, deposition of thin films takes place from aqueous solutions at low temperatures by a chemical reaction between dissolved precursors, with the help of a complexing agent. CBD has been used in the deposition of

semiconductor thin films for over forty years [32]. Among all techniques used to grow Group II-VI semiconductors, CBD has the advantage of being a simple, low temperature, and inexpensive large-area deposition technique. CBD is presently attracting considerable attention as it does not require sophisticated instrumentation like vacuum system and other expensive equipments. The starting chemicals are commonly available and inexpensive. Using CBD, a large number of substrates can be coated in a single run. Unlike electroplating, electrical conductivity of the substrate is not a necessary requirement. Any insoluble surface to which the solution has a free access will be a suitable substrate for deposition, which makes CBD suitable for coating surfaces of any morphology and geometry. The low temperature deposition avoids oxidation and corrosion of metallic substrates. Chemical deposition results in almost pin hole free, uniform and even highly stoichiometric films since the basic building blocks are ions instead of atoms. The preparative parameters are easily controllable and better orientations and improved grain structure can be obtained [33]. CBD has been extensively used in growing group II-VI semiconductors, such as CdS, CdSe, CdO, HgS, HgSe, ZnS, ZnSe, and ZnO [34].

The deposition medium for CBD of "MX" thin films (M^{2+} is Group II metal while X^{2-} is Group VI chalcogenide) consists of one or more salts of Group II metal ion M^{2+} (Zn^{2+}, Cd^{2+}, or Hg^{2+}), a source for the chalcogenide X^{2-} (O^{2-}, S^{2-}, or Se^{2-}), and usually a complexing agent, in aqueous solution. The metal precursors / salts are expected to have moderate to high solubility in water, e.g., chlorides, iodides, acetates, nitrates, or sulfates. Chalcogenide sources typically include thiourea, thiosulfate, or thioacetamide for S^{2-} ions, and selenourea, selenosulfate, or N, N-dimethylselenourea for Se^{2-} ions, while the dissociation of water itself provides oxygen in the form of OH^{-} ions. The complexing agent provides ligands such as ammonia, ethanolamine, ethylenediamine, methylamine, dimethylamine, triethanolamine, hydrazine, tartrate, citrate, cyanide, etc.

Chemical bath deposition is believed to be based on the following steps [35]:

(1) Equilibrium between the complexing agent and water;

(2) Formation/dissociation of ionic metal-ligand complexes $[M(L)_i]^{2-ik}$, where L^{k-} denotes one or more ligands;

(3) Hydrolysis of the chalcogenide source;

(4) Formation of the wanted solid.

Most of the control of the CBD process resides in adjustment of the last three steps. Hydrolysis of the chalcogenide source (step 3) is critical because it provides the desired non-metal species that pull the metal cations out of solution to form the solid film. This step is highly sensitive to the solution's pH and temperature. The formation of the solid MX thin film (step 4) begins when the rising concentration of X^{2-} from step 3 causes the ionic product $[M^{2+}][X^{2-}]$ to exceed the solubility product of forming solid product. In practice, the central issue is whether the solid forms as a film or as particles dispersed in the liquid; and in the case of film formation, whether deposition proceeds by ion-by-ion growth on the substrate (heterogeneous reaction) or by adsorption and coagulation of colloids that were formed in the solution (homogeneous reaction). The formation of the metal ion complex (step 2) allows control over the rate of formation of solid metal hydroxides, which competes with step 4, which would otherwise occur immediately in the normally alkaline solutions. These steps together determine the composition, growth rate, microstructure, and topography of the resulting thin films [36].

2.5.1. Chemical Bath Deposition of CdS

Among all group II-VI semiconductors, chemical bath deposition of CdS is the most extensively investigated. Ammonium hydroxide is by far the most complexing agent that has been used in growing CdS thin films using CBD. It provides amine ligand which, when added to cadmium, forms cadmium tetraammine complex $Cd(NH_3)_4^{2+}$.

$$Cd^{2+} + 4NH_3 \Leftrightarrow Cd(NH_3)_4^{2+} \qquad (1)$$

The stability constant of cadmium tetraammine is [37]:

$$\beta = [Cd(NH_3)_4^{2+}] / [Cd^{2+}][NH_3]^4 = 10^{7.12} \qquad (2)$$

The formation of cadmium tetraammine complex in the solution ensures the slow release of Cd^{2+} ions so that $Cd(OH)_2$ will be formed at the solid liquid interface (substrate) and not in the solution itself; $Cd(OH)_2$ nuclei at the substrate will act as nucleation centers for CdS by adsorbing S^{2-} ions, thereby converting $Cd(OH)_2$ into CdS. It is widely believed that $Cd(OH)_2$ acts as a catalyst for decomposition of thiourea (the S^{2-} source). As a result, sulfide formation

will occur preferentially at the surface of the hydroxide layer on the substrate rather than nucleate separately in the solution. Once nucleation of CdS has begun on the substrate, it becomes easier for the film to grow. The crystals will continue to grow until the homogenous reaction dominates over the heterogeneous reaction which will result in the depletion of the Cd^{2+} and S^{2-} ions in the solution. In principle, the growth kinetics of CdS using ammonia can be explained on the basis of the following equations:

$$Cd^{2+} + 4NH_3 \leftrightarrow Cd(NH_3)_4^{2+} \quad (1.1)$$

$$NH_3 + H_2O \leftrightarrow NH_4^+ + OH^- \quad (1.2)$$

$$Cd^{2+} + 2OH^- \leftrightarrow Cd(OH)_2 \quad (1.3)$$

$$SC(NH_2)_2 + 2OH^- \leftrightarrow S^{2-} + 2H_2O + H_2CN_2 \quad (1.4)$$

$$Cd(OH)_2 + S^{2-} \leftrightarrow CdS + 2OH^- \quad (1.5)$$

The same methodology could be employed in CBD of other group II-VI semiconductor compounds, which facilitates the experimental search for optimum deposition conditions considerably.

2.6. Band alignment at buffer layer/absorber materials

2.6.1. Band discontinuity at heterojunction interface

Figure 5 shows a heterojunction band diagram, with the assumption that $E_{g1}>E_{g2}$. The vacuum level is everywhere parallel to the band edges and is continuous, and the discontinuity in conduction band edges ΔE_c and valence band edges ΔE_v will occur at the interfaces between the two materials due to the different band gaps [38]. The electronic band diagrams are determined by the band-gap energies, and the electron affinities of the individual layers. Depending on the relative magnitudes of electron affinity χ_1 and χ_2, the conduction-band minimum of layer 1 is above or below that of layer 2.

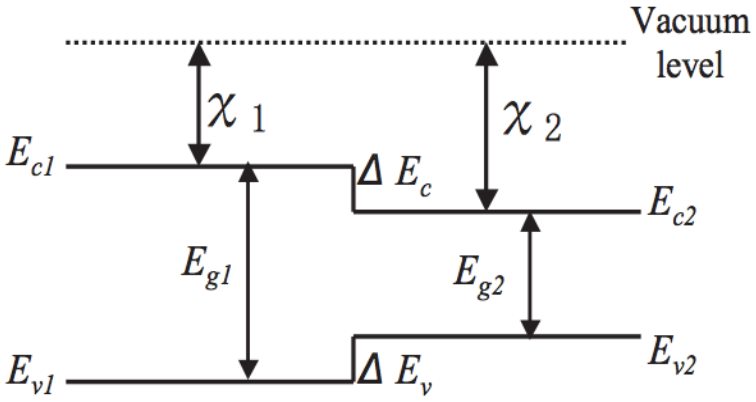

Figure 5. Band diagram of *p-n* heterojunction [38].

Depending upon the difference between electron affinity χ_1 and χ_2, we could have type I or type II heterojunction interfaces [39]. As shown in Figure 6, when conduction-band minimum (CBM) of layer 1 is above that of layer 2, and valence band maximum (VBM) of layer 1 is below that of layer 2, then the band alignment is of type I. On the other hand, if the both of CBM and VBM for layer 1 are below that of layer 2, the band alignment is of type II**.**

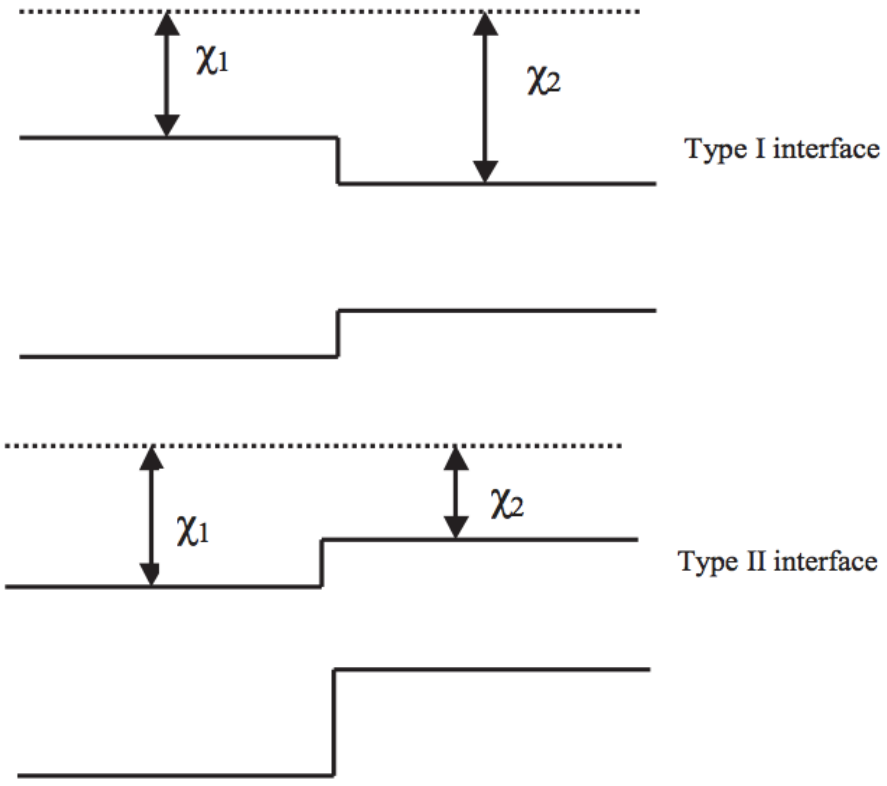

Figure 6. Type I and type II heterojunction interfaces [39].

Recalling that electrostatic potentials need to be added to the energies in band diagrams, the equilibrium band diagram is as shown below. Note that band bending that occurs inside the depletion regions reflecting the presence of an electric field and a corresponding electrostatic potential. Also note that the Fermi level in equilibrium is flat and constant throughout the device. The vacuum level also bends in response to the electric field, as shown in Figure. 7.

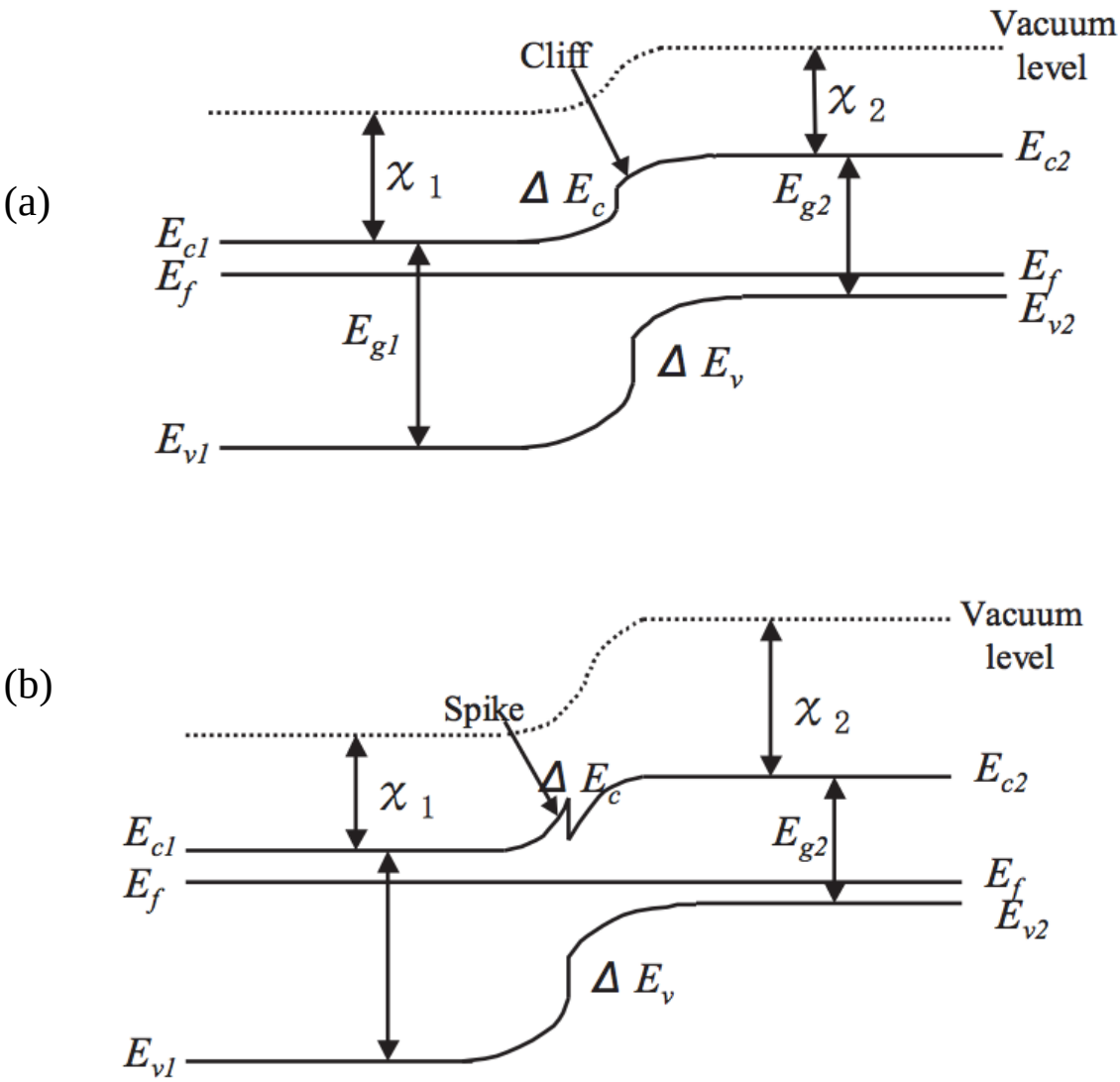

Figure 7. Band alignment of heterointerface considering electrostatic potentials.

(a): type I interface. (b): type II interface [40].

If there is a band offset it may lead to the formation of 'spike' or a 'cliff', depending on sign of the offset, as shown in Fig.7. (a) and (b). If the band offset produces a cliff, probability of the interface recombination of majority carriers is increased, and the flat band condition is achieved at bias smaller than E_g/q of the absorber [40]. One consequence is that output

voltage of the cell is limited in this case, because of the lack of barrier height. Band alignment with a moderate spike is rather optimal, although the presence of a large spike decreases the flow of the minority carrier.

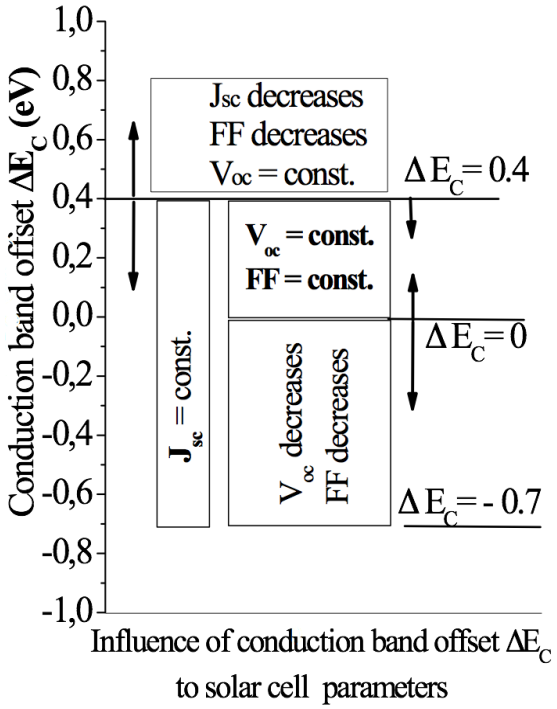

Figure 8. Influence of conduction band offset to solar cell parameters. Constructed on the base of data of [41].

The band alignment in the interface area has a great importance for solar cell performance, as shown by T. Minemoto et al. on the base of theoretical calculations [41] (see Figure 8).

The conduction band offset was varied from -0.7 to 0.6 eV. When the conduction band offset is in the range of -0.7-0.4 eV, short circuit current density *(J_{sc})* is nearly constant and that is over 0.4 eV, J_{sc} decreases abruptly. If the height of this barrier becomes over 0.4 eV, photo-generated electrons cannot cross over the barrier. Therefore, J_{sc} decreases abruptly. When the conduction band offset is in the range of -0.7-0 eV, open circuit voltage value (V_{oc}) decreases with increasing the absolute value of conduction band offset and reducing carrier lifetimes at the window/absorber interface. V_{oc} is nearly constant when the conduction band offset is over 0 eV. As the conduction band offset is in the range of 0-0.4 eV, fill factor *(FF)* is nearly constant. *FF* decreases abruptly when the conduction band offset is over 0.4 eV due to the formation of barrier against photo-generated electrons.

For the absorber/window heterostructure we can summarize: a large positive conduction band offset (ΔE_c) creates a spike, which acts like a barrier and obstructs the flow of photo generated carriers from the absorber to the buffer layer but theoretically, $0 \leq \Delta E_c \leq 0.4$ is optimal to obtain the reasonable efficiency from the solar cells. If $\Delta E_c < 0$, a cliff forms in the band structure, which allows interface recombination of carriers. Hence, open-circuit voltage in the solar cells decreases. It is predicted that $\Delta E_c = 0.2$ eV is an acceptable for good CZTS solar cells [42].

2.6.2. CdS/CZTS heterointerfaces

Theoretically, the conduction band offset of CdS/CZTS has been calculated to be negative, while the reported experimental values vary widely. For example, Chang Yan et al. report a cliff-like conduction band offset of -0.24 eV [43]. According to *p-n* junction band alignment simulation, when CBO is in the range of -0.7-0 eV, the V_{oc} and *FF* decrease abruptly. So the cliff-like CBO of CdS/CZTS is undesirable and is considered to be the main problem at heterojunction interface. A schema of estimated band alignment CdS/CZTS is plotted in Figure 9.

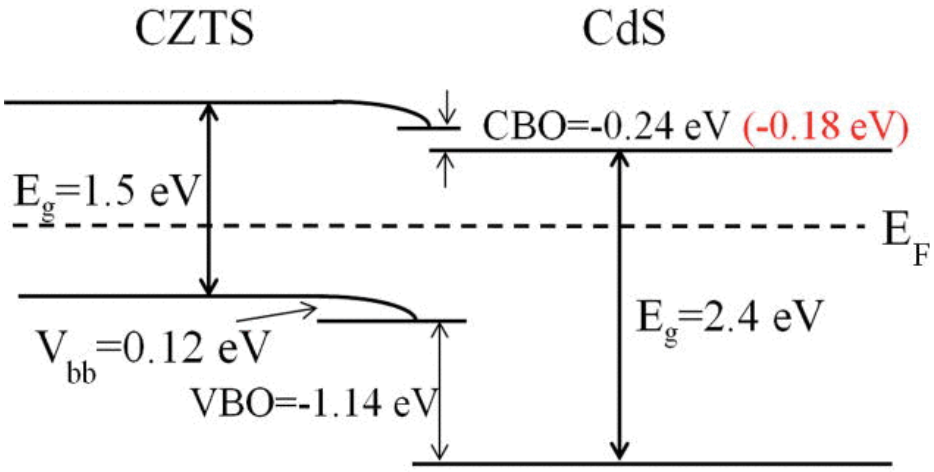

Figure 9. A schema of estimated band alignment CdS/CZTS [43].

2.6.3. In_2S_3/CZTS heterointerfaces

The investigator Chang Yan et al. calculated the CBO of In_2S_3/CZTS is 0.41 eV. According to *p-n* junction band alignment simulation, when CBO is higher than 0.4 eV, J_{sc} and *FF* decrease more abruptly and dramatically compared to those CBO value in the range of -0.7-0.4. This is largely due to the formation of a high barrier against photo-generated electrons. Compared

with the desired optimal CBO in the range of 0.0-0.3 eV [41], the spike-like CBO value of 0.41 eV obtained for In_2S_3/CZTS would result in such a barrier. A schema of estimated band alignment In_2S_3/CZTS is plotted in Figure 10.

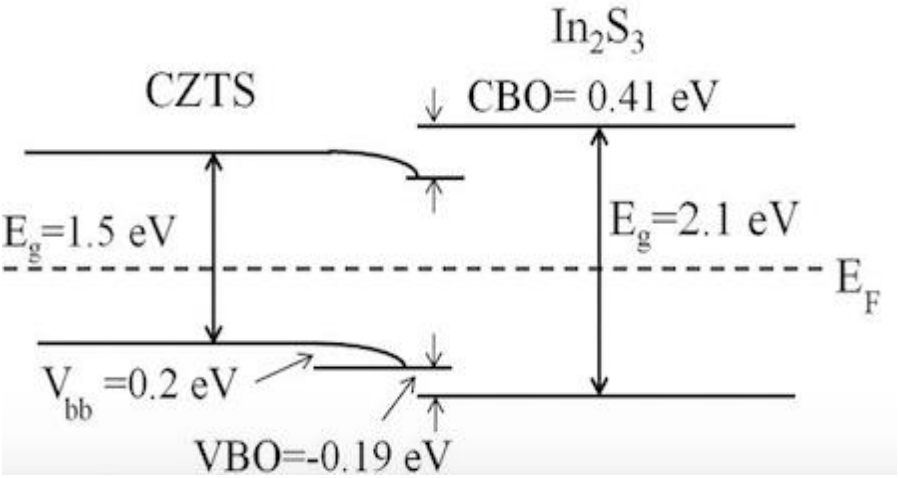

Figure 10. A schema of estimated band alignment In_2S_3/CZTS [43].

The fact that the CBO between CZTS and In_2S_3 is spike-like whilst that between CZTS and CdS is a cliff-like, it is possible that a CdS hybrid with In_2S_3 might allow to achieve an optimum spike-like CBO value in the range of 0-0.3 eV [43], which may demonstrate an overall superior V_{oc} and CZTS device performance.

2.7. Hybride buffer layer/CZTS

One of the limiting factors for CZTS solar cells' performance is the problem of CdS/CZTS interface recombination. In the study [41] CdS/In_2S_3 hybrid buffer was developed and applied onto CZTS solar cells based on considerations that In_2S_3 has a influence on CZTS solar cells because indium (In) as a dopant since: i) In may form both *p-type* doping in CZTS or *n-type* doping in CdS since it can substitute for Sn in CZTS (In_{Sn}) and for Cd in CdS (In_{Cd}), and ii) the formation energies of In_{Cd} and In_{Sn} defects are likely to be low, because In has a similar atomic radius to that of Cd or Sn and the ion charge of In^{3+} is only one remove from that of Cd^{2+} or Sn^{4+}. So In^{3+} diffusing into CZTS absorber and CdS layer can enhance the carrier concentration that lead to the improved solar cells performance [44]. Recently, IBM and Solar Frontier have reported high efficiency CZTSSe of 12.3% and CZTS of 9.2% respectively [45-46]. They both achieved high efficiency CZTSSe and CZTS solar cells by applying hybrid

buffer layer with combination of In_2S_3 buffer and CdS buffer. As for CZTS, the researchers at Solar Frontier claim that the hybrid buffer layer could reduce carrier recombination at the interface not only between the buffer and the absorber layers but also between i-ZnO and buffer layers. In terms of CZTSSe, researchers at IBM believe the improvement results from increased carrier concentration of CZTSSe by indium (In) doping. The schematic of double emitter (In_2S_3/CdS) solar cell structure studied is shown in Figure 11.

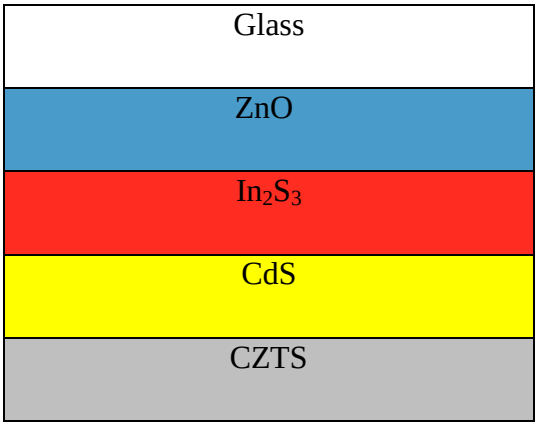

Figure 11. Schema of double emitter (In_2S_3/CdS) solar cell structure [46].

2.8. Summary of the literature review and the objective of study

CZTS is a I_2-II-IV-VI_4 group quaternary compound of kesterite structure and its band gap is about 1.5eV which is optimum energy band gap for solar energy conversion. Compared to crystalline silicon, CdTe and CIGS, CZTS are from earth abundant, non-toxic and environmentally friendly elements. So, CZTS could be the best candidate for thin film absorber material for the next generation thin film solar cells. Recently, it has been announced that CZTS type thin film solar cells have already reached more than 12.6% efficiency based on sulfo-selenide CZTSSe material. But there still exists a large performance gap between the CZTS and the more developed CIGS cells that currently have efficiencies of over 21%, which is mainly due to high V_{oc} deficit of CZTS cells. The main reason responsible for the high V_{oc} deficit in CZTS solar cells is believed to be the charge pair recombination in both the CZTS bulk and at the CZTS/CdS interface. The CBO of CZTS/CdS is cliff-like, which is undesirable and is considered to be the main problem at the heterojunction interface that is limiting the V_{oc} values. While CBO of CZTS/In_2S_3 is spike-like, the combination of In_2S_3 with CdS as a hybrid buffer is a promising choice for CZTS solar cells because the conduction band alignment can be more favorable at the CZTS/(CdS-In_2S_3) interface.

The focus of this work is to modify 1) the Cd^{2+} ion source for CdS deposition with the aim to find the optimal Cd^{2+} reagent; and 2) the deposition time to find the optimum time for CdS deposition. Due to the non-ideal band alignment at the CdS/CZTS interface, particularly the conduction band alignment plays a crucial role for the electron transport towards the front contact [7], we are focused also to 3) the effect of In_2S_3/CdS hybrid buffer layer to the CZTS monograin layer (MGL) solar cells' performance and 4) to the effect of annealing treatment with the aim to improve the imperfections at absorber/buffer interface.

3. Experimental

3.1. Chemical deposition of buffer layers

3.1.1. Experimental set-up

A typical set-up for CBD deposition is shown in Figure 12: a beaker filled with aqueous solution of precursors for deposition is in a water bath placed on a hot plate that controls temperature and stirring process. The substrate is immersed into the solution and kept there for a determined time period. Stirring is continuous from room temperature. The beaker with solution is covered with a cap to avoid evaporation of ammonia.

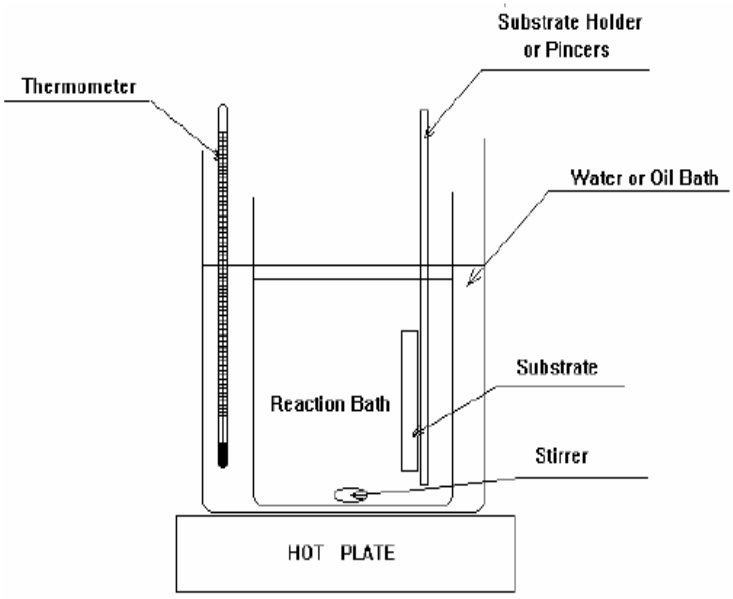

Figure 12. Schematic of Chemical bath deposition set-up.

3.1.2. Experimental procedure

CdS and In-S films were deposited onto bare glasses, Mo and ITO covered glasses and on CZTS monograin membranes for different time with the aim to study the film evolution and to find out the rate of deposition process.

Cleaning and degreasing of substrates guarantees successful chemical deposition process of thin films. Glass and ITO glasses were cleaned with sulphuric acid (conc. H_2SO_4) at 60 ^oC for

10 minutes and rinsed with deionized water, and ITO substrates were activated in a mixture of $HCl+HNO_3$ [47] for few seconds followed by rinsing.

For the CZTS membranes, prior to chemical deposition of CdS, the membranes were etched with 1% Br_2-methanol solution for 5 seconds followed by etching with 10% KCN+1% KOH solution for 5 seconds. This chemical treatment has shown a positive effect to solar cell parameters [48]. The presence of ZnS and Sn-S secondary phases is favored by Zn-rich and Cu-poor synthesis conditions that are required to obtain device-grade absorber layers. Several chemical etching processes based on the use of 1% Br_2-methanol and 10% KCN+1% KOH have been developed to remove undesired Sn-S, Cu_2SnS_3 and Cu_xS binary phases to activate the interface of solar cells with the aim to improve the efficiency of CZTS-based solar cells [49-50].

3.1.3. Deposition of CBD-CdS/In_2S_3 thin film

CdS and In_2S_3 films were deposited on glass substrates, glass/ITO substrates and absorber material (CZTS) monograin membranes by chemical bath deposition with the aim to study the optimal conditions for CdS and In_2S_3 deposition and in order to compare the influence of CdS and In_2S_3 deposition time to CZTS solar cell characteristics. The precursor solutions for cadmium sulphide chemical bath solution were $Cd(NO_3)_2$ (0.01M), NH_4OH (2M) and TU (1M). For CdS deposition 21 ml of CdI_2 solution, 21 ml of TU solution and 80 ml of ammonia was mixed with 30 ml of deionized water (see Tabel 1). pH of solution was pH=11.2. The precursor solutions for chemical deposition of indium sulphide were 2M $InCl_3$, 1M TAA. Two recipes were used for In_2S_3 deposition. By recipe 1, 1.25 ml of $InCl_3$ solution and 35 ml of TAA solution was mixed with 63.75 ml deionized water (see Table 2). In the recipe 2, citric acid was used as complexant. For In_2S_3 deposition by recipe 2, 1.25 ml of 2M $InCl_3$ solution, 35 ml of 1M TAA solution and 10 ml of 1M citric acid solution was mixed with 53.75 ml deionized water (see Table 3). The pH value of solution was adjusted to 2.5 by adding sodium hydroxide and hydrochloric acid [51]. CdS was deposited at 45 °C and In_2S_3 at 70 °C, temperature was kept constant [52]. CdS and In_2S_3 deposition time was varied. After finishing the deposition, the substrates were rinsed thoroughly with distilled water and dried by nitrogen gas. The buffer layers were then subjected to annealing at 120-160 °C in air.

Table 1. The precursor solutions for cadmium sulphide chemical bath deposition

Precursor solutions	Concentration, mol/L	Volume for 100 ml of deposition solution, ml	General conc. in deposition solution, mol/L
Cd^{2+} solution	0.01	14	0.0014
NH_4OH	2	52.5	1.05
Thiourea ($SC(NH_2)_2$)	1	14	0.07
H_2O		19.5	

Table 2. The precursor solutions for (fast) indium sulphide chemical bath deposition

Precursor solutions	Concentration, mol/L	Volume for 100ml of deposition solution, ml	General conc. in deposition solution mol/L
$InCl_3$	0.5	5	0.025
Thioacetamide (TAA)	1	35	0.35
H_2O		60	

Table 3. The precursor solution for (slow) indium sulphide chemical bath solution

Precursor solutions	Concentration, mol/L	Volume of 100ml for deposition solution, ml	General conc. in deposition solution mol/L
$InCl_3$	0.5	5	0.025
Thioacetamide (TAA)	1	35	0.35
Citric acid	1	10	0.1
H_2O		50	

3.2. Characterization methods

Table 4. Methods used for characterization of CdS, In_2S_3 thin films and solar cells

Charaterization methods	Properties	Operator
SEM	Morphology, thickness, grain size	PhD Valdek Mikli
XRD	Phase composition	PhD Rainer Traksmaa
PL	Band gap, impurity composition	PhD Taavi Raadik
EDX	Elemental composition	PhD Valdek Mikli
I-V measurement	Solar cell characteristics	Author of Thesis Sha Li

3.2.1. *I-V* characteristics of solar cells

In Figure 13 there are presented *I-V* characteristic curves of an ideal diode in the non-illuminated and illuminated conditions. When the current and voltage are negative, the diode consumes power supplied by the external circuit; on the contrary, if the diode is operated in the fourth quadrant, it will supply power to an external circuit, which is the basic working principle of solar cell device.

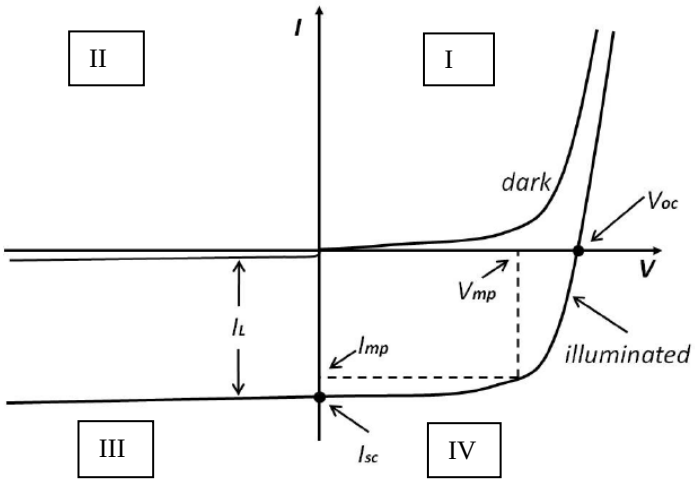

Figure 13. The graph of the *I-V* characteristics of an ideal diode solar cell for non-illuminated (dark) and illuminated states [53].

Thus, for a solar cell the equivalent circuit shown in Figure 14 may be used. Photocurrent I_L supplied by the current source, R_S represents the series resistance of all stacks of constituent layers of solar cell: the resistance of absorber layer and resistance of the electrode materials layers. The smaller is the value of R_S, the better is the performance of solar cell. R_{SH} is equivalent to shunt resistance of solar cells, the bigger value of R_{SH} is more favorable, the performance of solar cells is more excellent.

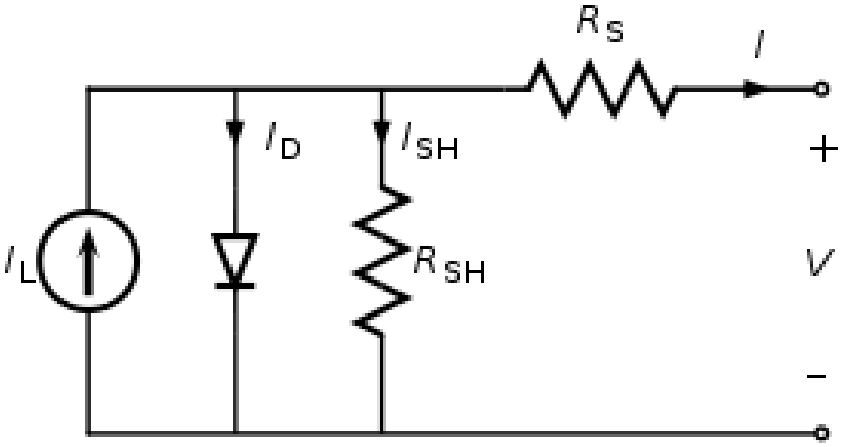

Figure 14. Equivalent electric circuit of solar cell [54].

For simplicity, assume that the photocurrent can be superimposed on the dark current, and assumes R_S and R_{SH} are 0 and ∞, respectively (ideal situation). The current density J can be expressed as:

$$J = J_0 \left[\exp\left(\frac{\mathrm{qV}}{mk\mathrm{T}} - 1\right)\right] - J_L \quad (1)$$

J_0 is referred to reverse saturation current, J_L is referred to photogenerated current. Representitives of good or bad performance of the solar cell important parameters are short circuit current (I_{sc}), open circuit voltage (V_{oc}), fill factor (FF), efficiency (η) and maximum power (P_{max}). Here are explanations about these parameters. Short-circuit current is photogenerated current, which flows under light conditions through the two connected terminals of the solar cell. Open circuit voltage is represented when two terminals of the solar cell are disconnected, ie $J = 0$. Therefore, the open circuit voltage is expressed as:

$$Voc = \frac{mk\mathrm{T}}{\mathrm{q}} \ln\left(\frac{J_L}{J_0} + 1\right) \quad (2)$$

When a point on the curve corresponding to the product of maximum power current and the maximum power voltage. The point is called maximum power point. From this we can get the formula for fill factor and conversion efficiency:

$$FF = \frac{Imax * Vmax}{Isc * Voc} \qquad (3)$$

$$\eta = \frac{Pmax}{Prad} \qquad (4)$$

P_{rad} represents the power of solar radiation. Standard conditions for the characterization of solar cell performance are as follows: the power density of the incident light is 100 mW / cm^2, AM1.5 spectral criteria, measurement temperature is 25℃.

4. RESULTS AND DISCUSSIONS

4.1. Influence of different Cd salts as Cd^{2+} sources for CdS deposition on CZTS/CdS MGL solar cell characteristics

4.1.1. Characterisation of CdS layers on glass

For CZTS/CdS solar cells CdS was deposited onto uniform pieces cut from CZTS membranes for 30 min at 45°C. Cd^{2+} source was varied using different Cd salts (CdI_2, $CdCl_2$, $CdSO_4$, $CdAc_2$, $Cd(NO_3)_2$, $CdSO_4$+$InCl_3$). For elemental composition measurements and for electrical characterization, also for photoluminescence (PL) measurements CdS layers from different used Cd salts were deposited onto bare glass substrates as repeatedly stacked for 7 times, each time for 40 min at 45°C. These repeatedly covered glass substrates with CdS were annealed for 40 min at 350°C.

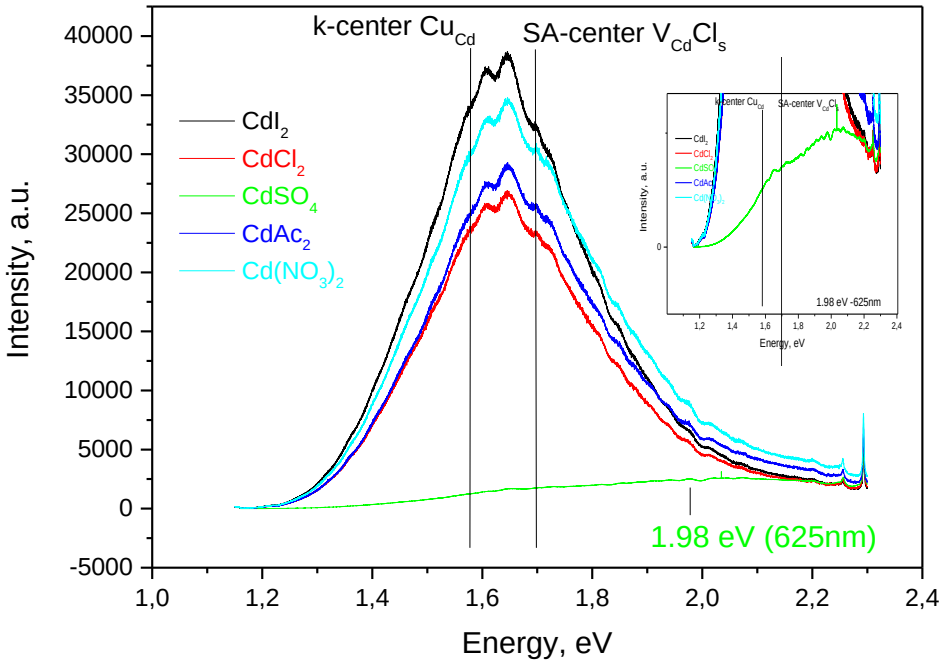

Figure 15. PL spectra of CdS layers deposited from different Cd^{2+} sources on glass, annealed in air at 350 C for 40 minutes. The positions of well-known PL peaks from self-activated (SA) and k-recombination channels are marked as vertical lines.

PL spectra of CdS layers on glass from different Cd^{2+} sources are shown in Figure 15. The CdS layers from cadmium iodide and cadmium nitrate have the highest PL intensity. All the spectra show a broad band with probably two components of so-called self-activated PL band in the vicinity of 1.7 eV and a shoulder at about 1.58 eV. The only exception is the PL spectrum of CdS layer deposited from $CdSO_4$ containing solution that has much lower intensity and has maximum in the vicinity of 2 eV (see insertion in Figure 15). The bright PL can be a sign of impurities in precursor salts.

. Table 5. Element composition of CdS layers determined by EDX

Used Cd-salt	CdI_2	$CdCl_2$	$CdSO_4$	$CdAc_2$	$Cd(NO_3)_2$
Concentration of Cadmium, at%	50.6	50.3	50.1	50.3	50.1
Concentration of Sulfur, at%	49.4	49.7	49.9	49.7	49.9

The element composition of CdS layers determined by EDX method is shown in the Table 5. It can be seen that all the CdS thin layers deposited from different Cd^{2+} sources are almost stoichiometric CdS. No other elements were detected by the EDX method. The ratio of Cd to S is very close to 1:1. The electrical resistivity of all annealed CdS films on glass was measured at room temperature using the two probe technique. For this purpose two parllel lines of liquid In–Ga eutectic mixture were painted onto the films keeping the distance between them constant. The CdS layers were highly resistive, showing resistivity over $2*10^9$ Ohm/cm^2.

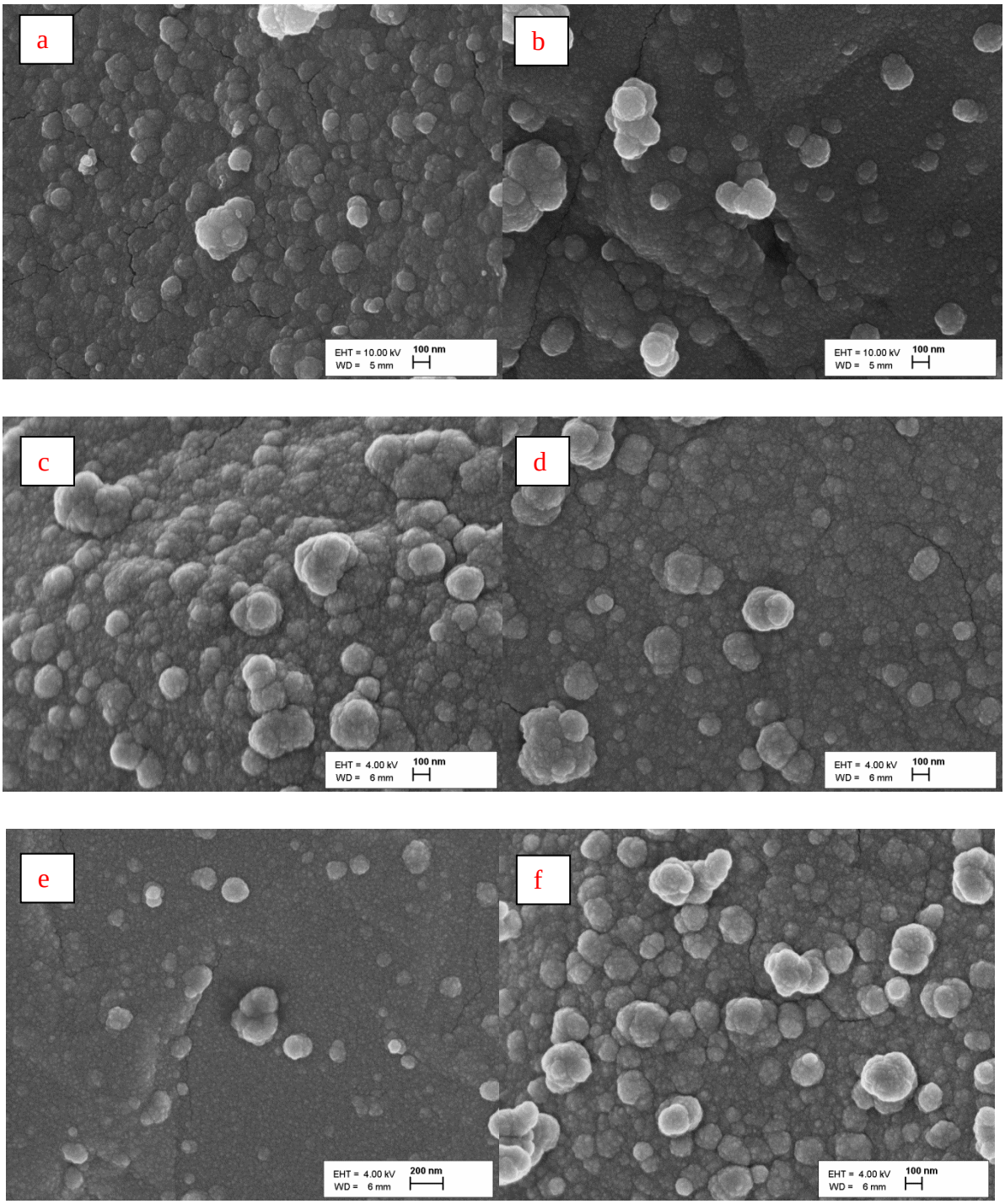

Figure 16. SEM images of CdS deposited with varied different Cd salts: a) CdI_2; b) $CdCl_2$; c) $CdSO_4$; d) $CdAc_2$; e) $Cd(NO_3)_2$; f) $CdSO_4$+$InCl_3$.

The morphology of CdS layers determined by SEM method is shown in the Figure 16. The coverage of CdS on CZTS grains was continuous, uniform. There are some big colloidal particles on the surface, but when using $Cd(NO_3)_2$ as the CdS deposition source, the size of grain is smaller and less big colloidal particles.

4.1.2. Characterization of CZTS/CdS MGL solar cells

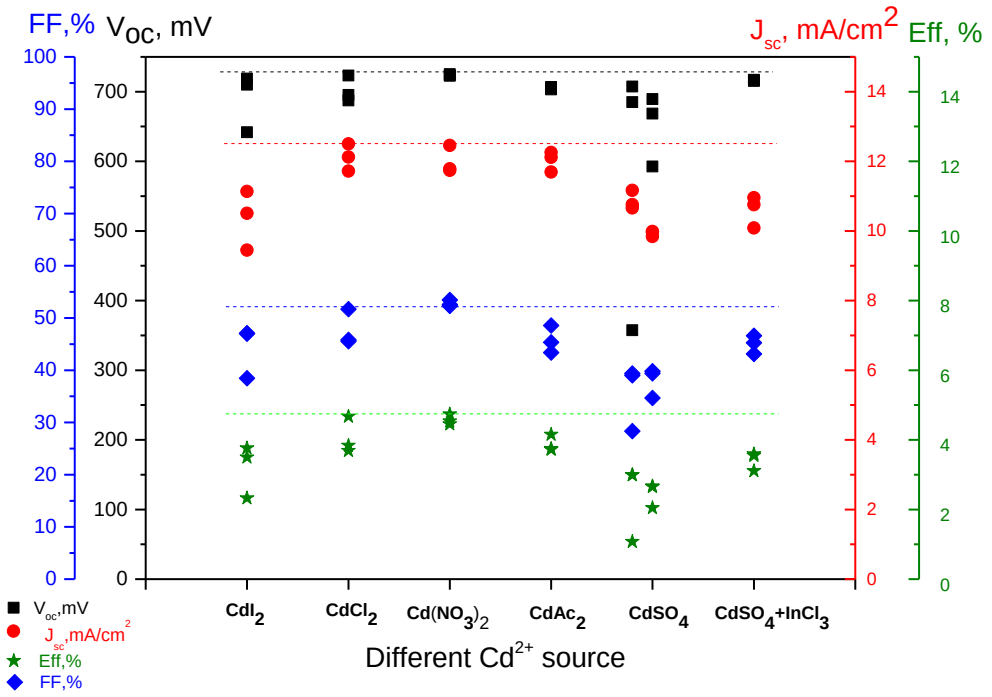

Figure 17. Characteristics of CZTS MGL solar cells with CdS buffer layers deposited from different Cd^{2+} sources.

The CZTS/CdS solar cells characteristics are shown in the Figure 17. The V_{oc} values are almost the same for every Cd-salt with the value of 710 mV. The J_{sc} and *FF* values vary with different Cd^{2+} sources. As the thickness of CdS layers from different Cd^{2+} sources vary also, and thickness has a big influence on the carrier flow that limits the J_{sc} value. So, the performances of solar cells with CdS layers from different Cd-salts are a little bit different. The highest solar cell performance and the smallest deviation of parameters have the solar cell with CdS from cadmium nitrate. Also, the coverage of CdS on CZTS grains was continuous, uniform, with small particles when $Cd(NO_3)_2$ was used as cadmium ion source (see Figure 16). Therefore we decided to use $Cd(NO_3)_2$ as Cd^{2+} source for CdS deposition in the following part of study.

4.2. Influence of CdS deposition time on CZTS/CdS MGL solar cells' characteristics

CdS deposition time was varied from 5-40 min at 45 °C using $Cd(NO_3)_2$ as Cd^{2+} source. This experiment was done to clarify the optimal deposition time for the CdS deposition onto CZTS

membranes and to see the influence on CZTS/CdS MGL solar cells performance. As deposited CdS film thickness was measured by SEM cross-sectional images and the results are given in Figure 18. The morphology and thickness analysis was done to compare the film growth on different substrates also.

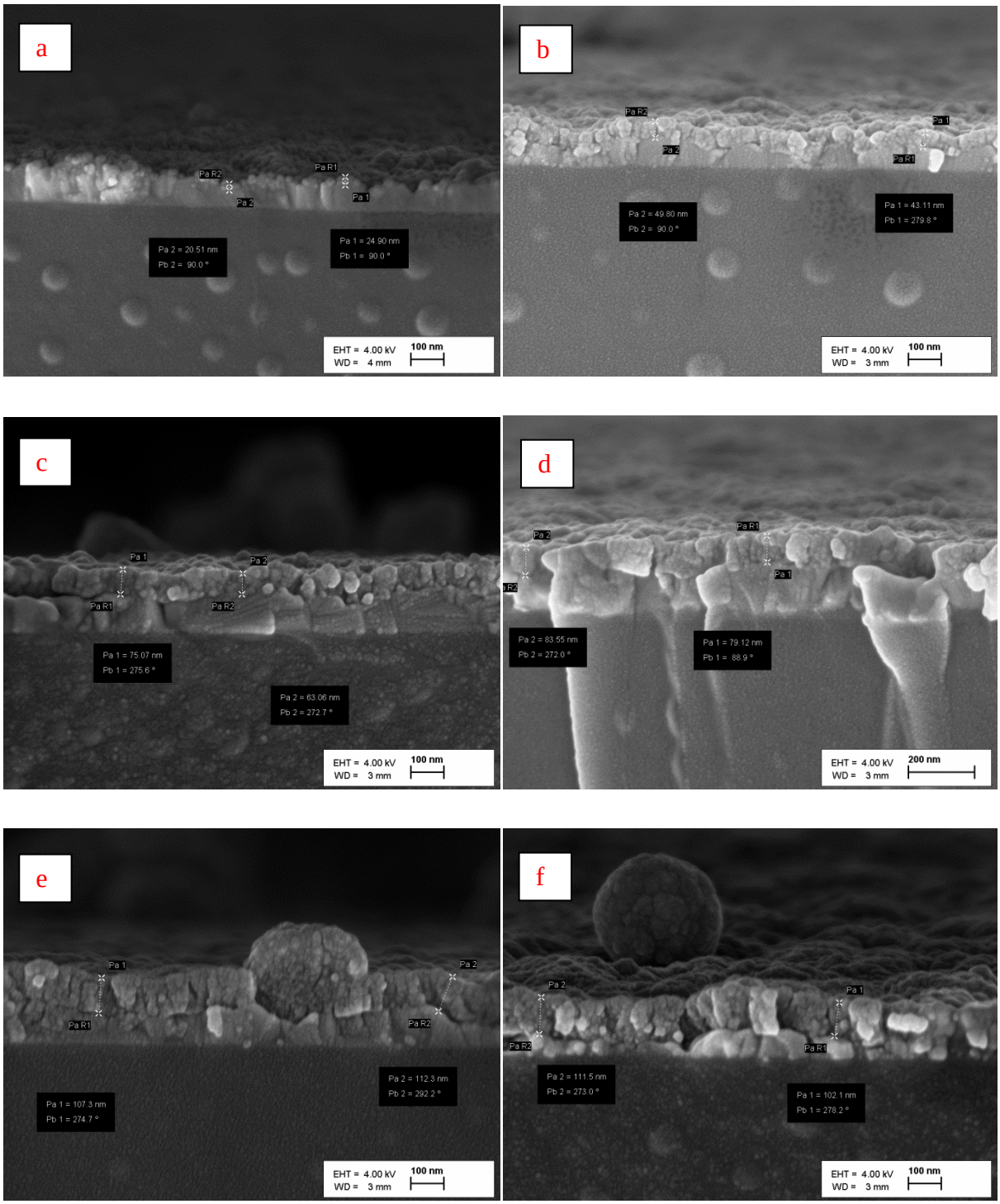

Figure 18. Cross-sectional SEM images of CdS films deposited with varied deposition time: a) 5 min;b) 10 min; c) 15 min; d) 20 min; e) 30 min; f) 40 min.

Figure 18 shows cross sectional SEM images of CdS films deposited for different time. It is noticable that the thickness of CdS layer increases by extending the CdS deposition time. In the short time deposition for 5 min, the CdS does not fully cover the substrate. After 10 min, all the substrates are fully covered with continuous CdS layer. There can be seen also big colloidal particles on the surface.

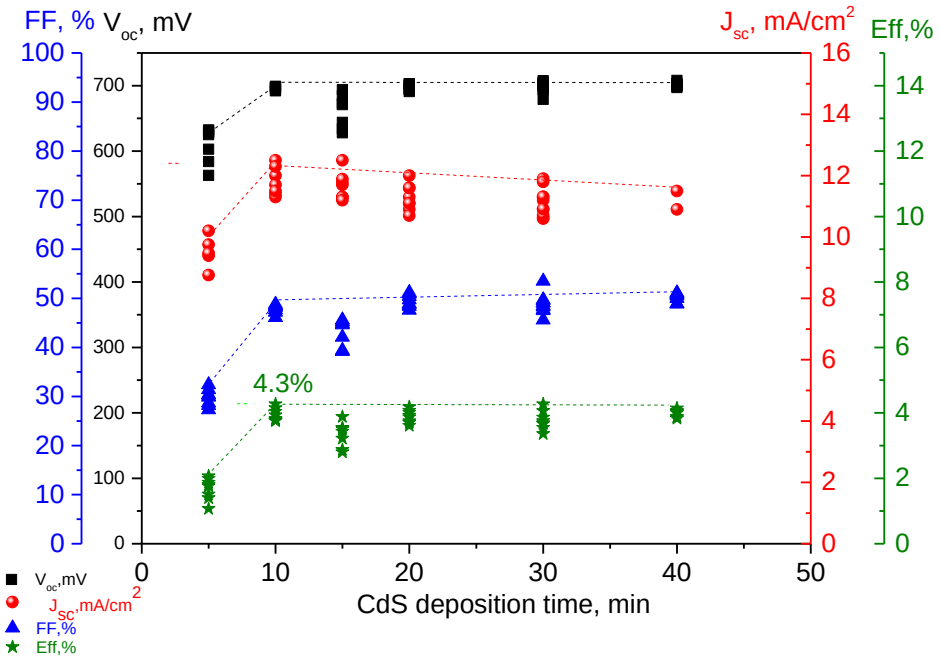

Figure 19. CZTS/CdS monograin membrane solar cell characteristic versus CdS deposition time. $Cd(NO_3)_2$ as Cd^{2+} source was used for CdS deposition at 45 °C.

Figure 19 shows the influence of CdS deposition time on the characteristics of CdS/CZTS MGL solar cells. This experiment was done to clarify the optimum conditions for the depositions of continuous and pin-hole free CdS layers by the used recipe. By increasing deposition time from 5 min to 10 min, it is seen that all solar cell parameters have improved. After the deposition of CdS for 10-15 min, the thickness of CdS layer increased with increasing deposition time and it led the increased Rs values. So the current density started to decrease when the CdS deposition time increased over 15 minutes. At the same time the V_{oc} and *FF* values stayed at constant level being around 700 mV and 50% respectively. The efficiency didn't improve with extended deposition time. In conclusion we can say that 10 min is enough time for CdS buffer layer deposition for CZTS MGL solar cells when the deposition temperature is 45 °C and $Cd(NO_3)_2$ is used as the Cd^{2+} source.

4.3. Influence of In_2S_3 buffer layer application for CZTS MGL solar cells

In_2S_3 films were deposited on CZTS absorber material at 70 °C for different deposition time and by different recipes. For recipe 1, showed in the Table 2 that is without citric acid, the deposition time was varied from 10-60 min. For recipe 2, showed in the Table 3 that is with added citric acid, the deposition time was varied from 20-90 min. pH value was kept constant around 2.5. The measured solar cells characteristics are shown in the Figure 20 and 21.

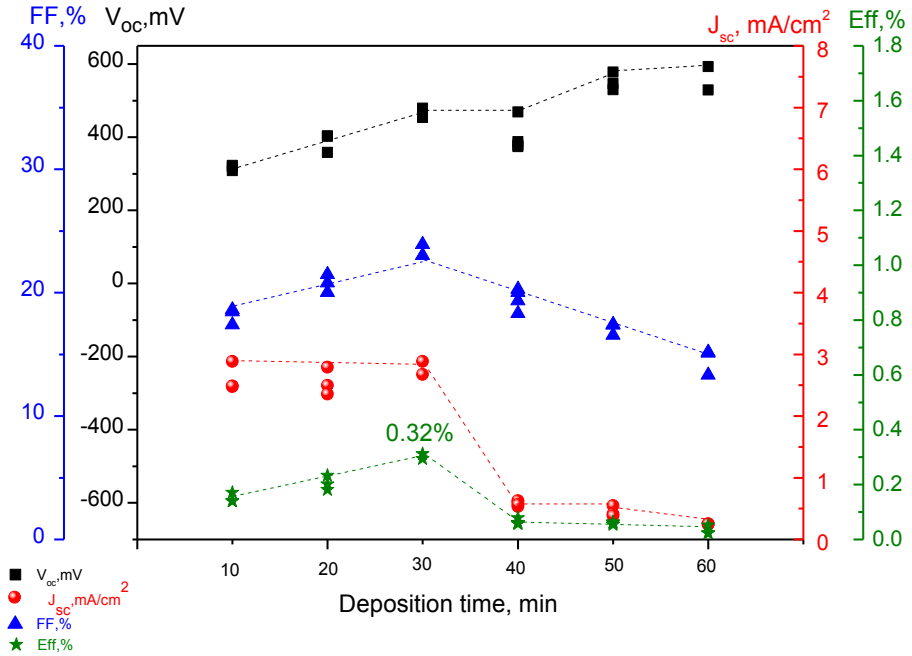

Figure 20. In_2S_3/ CZTS monograin membrane solar cell characteristic versus In_2S_3 deposition time. In_2S_3 was deposited at 70 °C used recipe 1 (without citric acid).

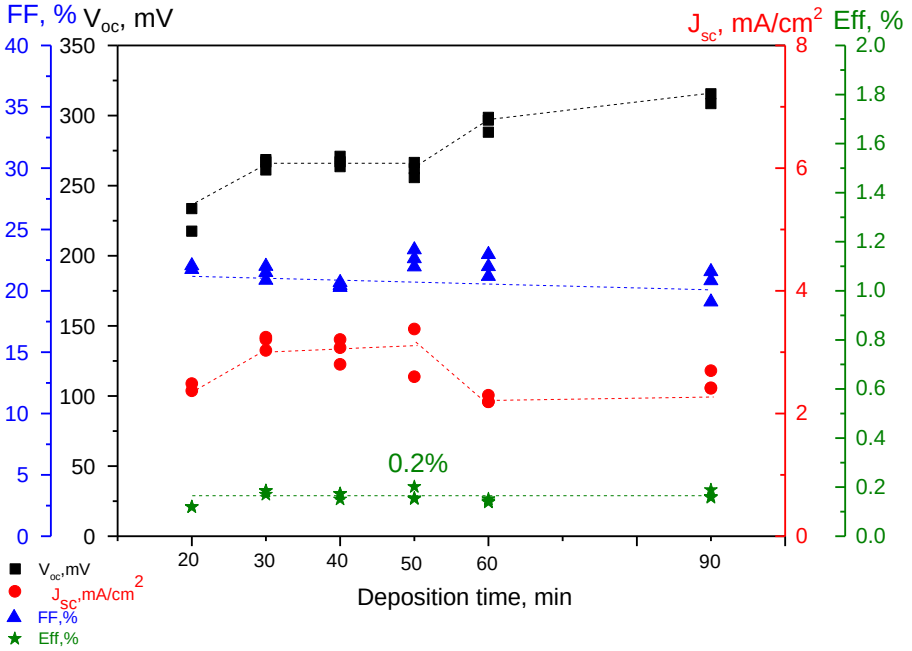

Figure 21. In_2S_3/ CZTS monograin membrane solar cell characteristic versus In_2S_3 deposition time for In_2S_3 deposition temperature 70 °C used recipe 2 (with citric acid).

From the Figure 20 and 21, it is clearly demonstrated that the V_{oc} increased by extending In_2S_3 deposition time. But the value of V_{oc} was much lower if compared to CdS/CZTS solar cells. Whatever used recipe 1 and recipe 2, the *FF* and J_{sc} was relatively low. So the performance of solar cells was extremely bad. The efficiency was much below 1% and the highest efficiency is around 0.32%. This result indicates that there might be a barrier for hole and/or electron transportation. Probably due to a junction property of In_2S_3/CZTS interface, that is much worse than that of CdS/CZTS interface [55].

4.4. Influence of CdS/In_2S_3 stacked buffer layer on CZTS MGL solar cells' characteristics

4.4.1. Influence of In_2S_3 deposition time on CZTS/CdS/In_2S_3 solar cell performance

First, CdS film was deposited onto the membranes of CZTS absorber material at 45 ˚C for 10 min, the composition of chemical solution is given in Table 1 (see part 3.1.3). After the chemical deposition of CdS, In_2S_3 film was deposited onto CdS-covered CZTS membranes at 70 ˚C for different deposition time (10, 20, 30, 40, 50, 60 min). The compositions of chemical

solutions are given in Table 2 and Table 3. Experimental details were described in the part 3.1.3.

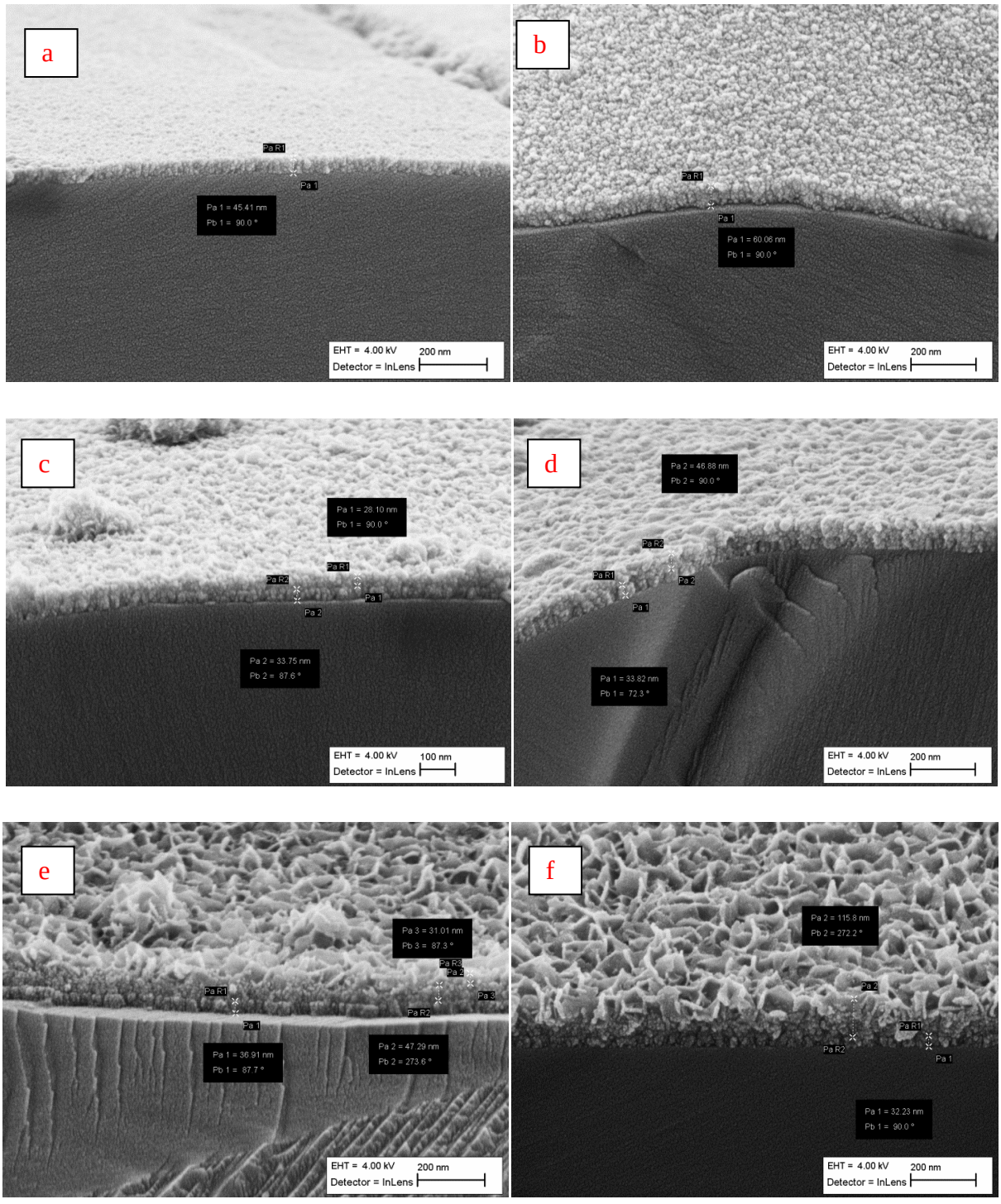

Figure 22. Cross-sectional SEM images of In_2S_3/CdS hybrid buffer layers with varied In_2S_3 deposition time: a) 10 min;b) 20 min; c) 30 min; d) 40 min; e) 50 min; f) 60 min; recipe 1 was used (without citric acid).

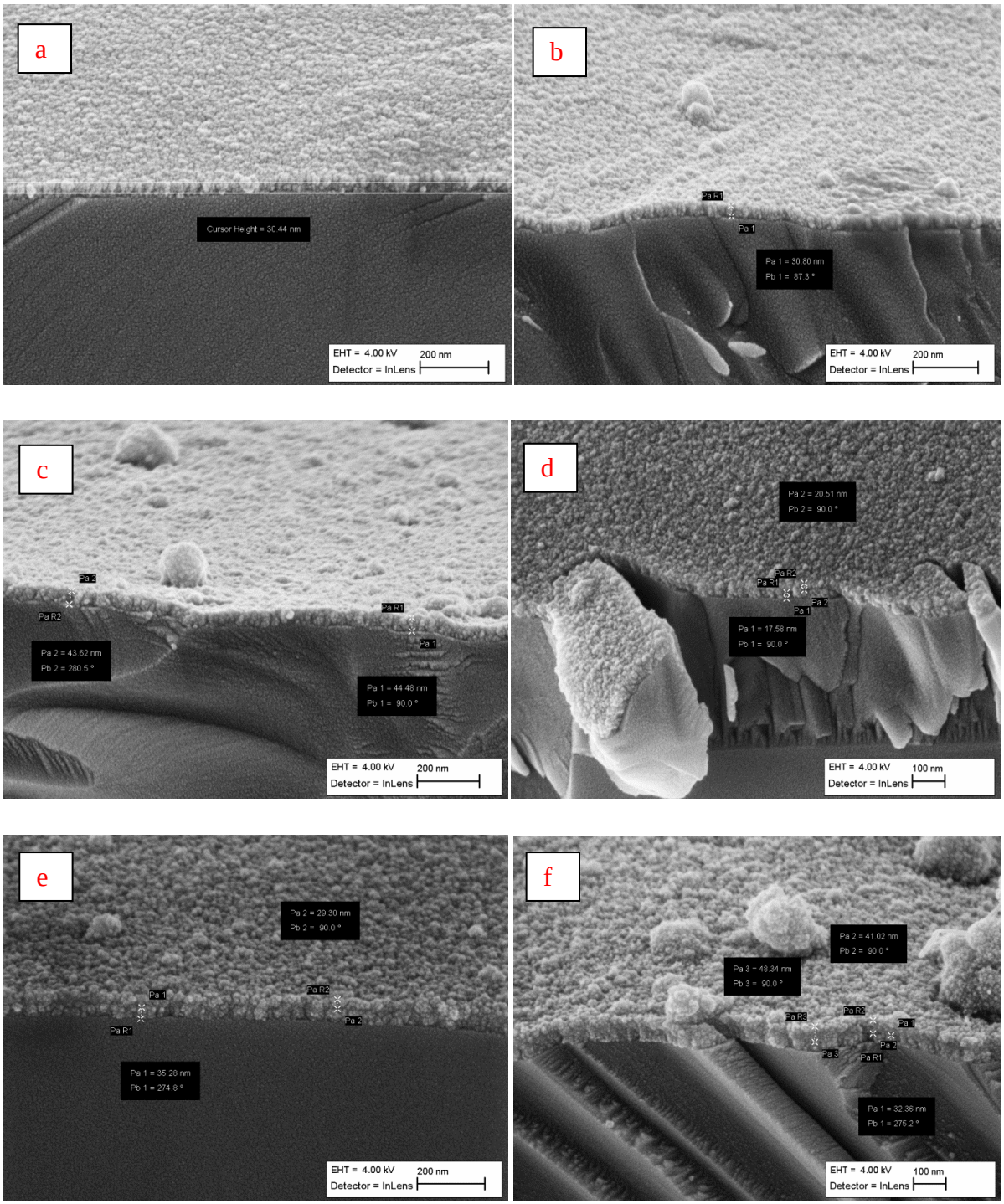

Figure 23. Cross-sectional SEM images of In_2S_3/CdS hybrid buffer layers with varied In_2S_3 deposition time: a) 10min; b) 20min; c) 30min; d) 40min; e) 50min; f) 60min; recipe 2 was used (with citric acid).

Figures 22 and 23 show the thickness and morphology of hybrid buffer layer on CZTS membranes. We can easily see that there is double layer on the CZTS membrane and that In_2S_3 film on the top of CdS film is fully covering the surface. The In_2S_3 films are following

the topography of CdS particles. The comparison of SEM images revealed that the thickness of hybrid buffer layer increased by increasing the In_2S_3 deposition time. For the recipe 1, with increased In_2S_3 deposition time 50-60 min, the morphology of In_2S_3 is flower like. For the recipe 2, the morphology of In_2S_3 is different. If compared layer thickness of recipe 1 with recipe 2, the thickness of In_2S_3 from recipe 1 is much thicker at the same In_2S_3 deposition time. This is because of the added citric acid into the precursor solution, that forms complex with In ions and the deliberation of indium ions from complex ions is inhibited. It slows down the growth rate of In_2S_3 layer. There can be seen also some big colloidal In_2S_3 particles on the film surfaces. The colloidal particles can be easily removed by ultrasonic agitation.

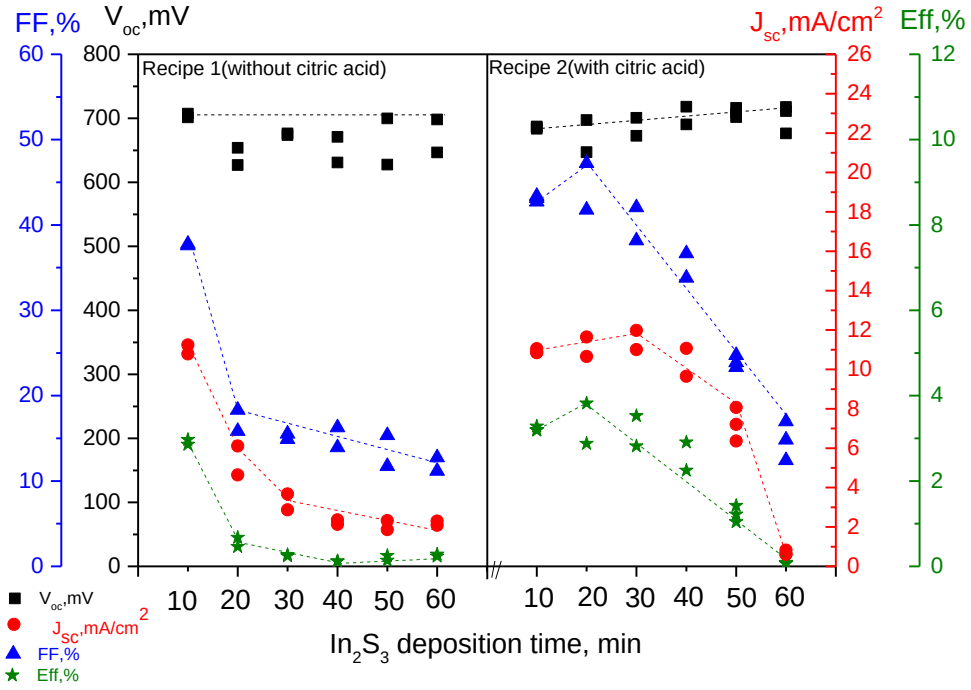

Figure 24. CZTS/(CdS-In_2S_3) monograin membrane solar cell characteristic versus In_2S_3 deposition time. CdS deposition time is constant.

Figure 24, shows the influence of In_2S_3 deposition time (thickness) on In_2S_3/CdS/CZTS-MGL solar cells' parameters. This experiment was done to clarify the optimal conditions for In_2S_3 deposition applied to In_2S_3/CdS/CZTS-based solar cells. For recipe 1 (without citric acid) shown in the left part of graph, the J_{sc} and *FF* drop abruptly after 10 min. Due to this the efficiency of solar cells decreased by increasing In_2S_3 deposition time. For recipe 2 (with citric acid) shown in the right part of graph, the V_{oc} increased with extending In_2S_3 deposition time from 10-60 min. J_{sc} and *FF* raised up by 10-20 min then dropped abruptly. So, the

efficiency of solar cells increased from 10-20 min then decreased. The two different recipes showed different results that may be due to thickness and composition of In_2S_3 gained from different recipes. In conclusion, 20 min is the optimal deposition time for In_2S_3 deposition using recipe 2 (with citric acid) for In_2S_3/CdS/CZTS solar cells. So in the following part we used 20 min In_2S_3 deposition to continue studying the influence of CdS deposition time and annealing treatment for In_2S_3/CdS/CZTS-based solar cells. Afterwards, for recipe 1 (without citric acid), there should be find out the optimal deposition regime for In_2S_3/CdS/CZTS-based solar cells.

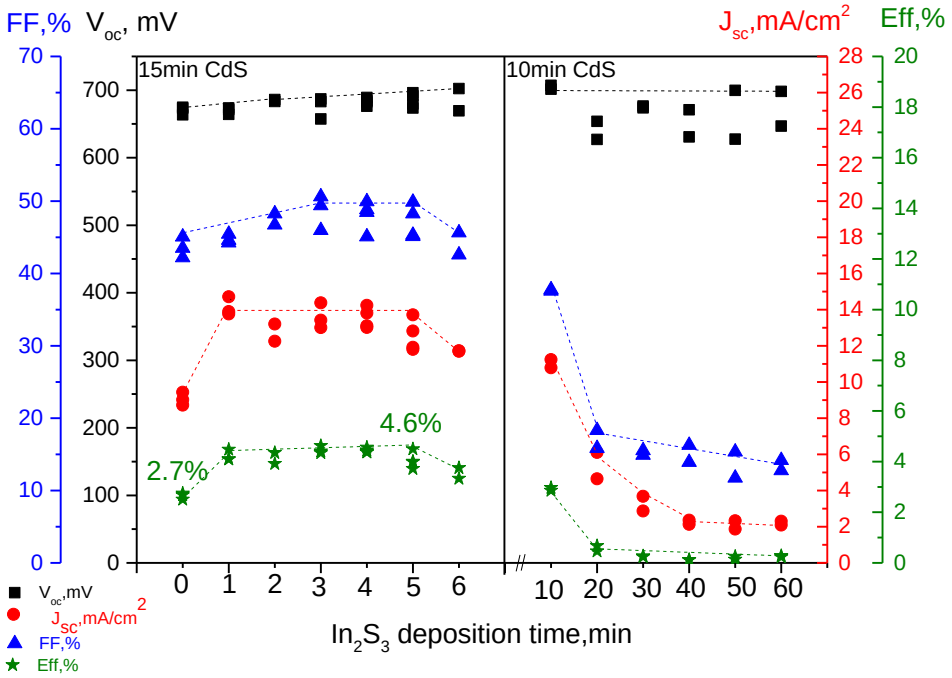

Figure 25. CZTS/CdS/In_2S_3 monograin membrane solar cell characteristic versus In_2S_3 deposition time by recipe 1 . CdS deposition time is constant.

Figure 25 shows the *I-V* characteristics of the cells, namely the open circuit voltage (V_{oc}), the short-circuit current density (J_{sc}), the fill factor (*FF*) and the efficiency (η). In order to find the optimal In_2S_3 deposition time by recipe 1 (without citric acid) for In_2S_3/CdS/CZTS-based solar cells, we deposited short time (from 1-6 min) In_2S_3 onto CdS/CZTS membranes (see left part of Figure 25). The CdS deposition time was 15 min. From the Figure 25, it could be seen that by increasing the In_2S_3 deposition time all the solar cells parameters increased first until 5 min of In_2S_3 deposition. After that with increased In_2S_3 deposition time, the current density and *FF* drop abruptly. This is because the increasing thickness of In_2S_3 will influence the series resistance value. When the thickness of In_2S_3 increased, the series resistance also

increased. Higher value of series resistance reduces the current through the load. The efficiency of solar cell also drops abruptly after 10 min. So the thickness of In_2S_3 has a great influence on the solar cell parameters and the thickness of In_2S_3 must be thinner. According to gained results, we made solar cells with hybrid buffer layer with short In_2S_3 deposition time from 0-6 min. From the Figure 25, the use of an In_2S_3/CdS double layer instead of a CdS single layer appreciably enhanced current density and *FF*. Finally, higher efficiency was achieved by the hybrid buffer. The V_{oc} didn't change a lot with increased In_2S_3 deposition time from 1-6 min. The current density also stayed constant from 1-5 min and then decreased after 6min. of In_2S_3 deposition time. *FF* increased with increasing In_2S_3 deposition time up to 3 min and then decreased after 5 min. So we can conclude that 5 min In_2S_3 deposition time is optimal time for hybrid buffer layer applied for CZTSMGL solar cell. The highest efficiency 4.6% was achieved when In_2S_3 deposition time was 5 min.

4.4.2. Influence of CdS deposition time on CZTS/CdS/In_2S_3 solar cell performance

In this part, we changed the CdS deposition time from 5-20 min using $Cd(NO_3)_2$ as the Cd^{2+} source in CdS deposition at 45 °C. Then In_2S_3 was deposited onto the CdS/CZTS films by using repice 1 (in Table 2) for 6 min and recipe 2 (in Table 3) for 20 min at 70 °C. Subsequently, the membranes were annealed for 10 min at 160 °C in air. The In_2S_3/CdS/CZTS solar cell characteristics are shown in the Figure 26.

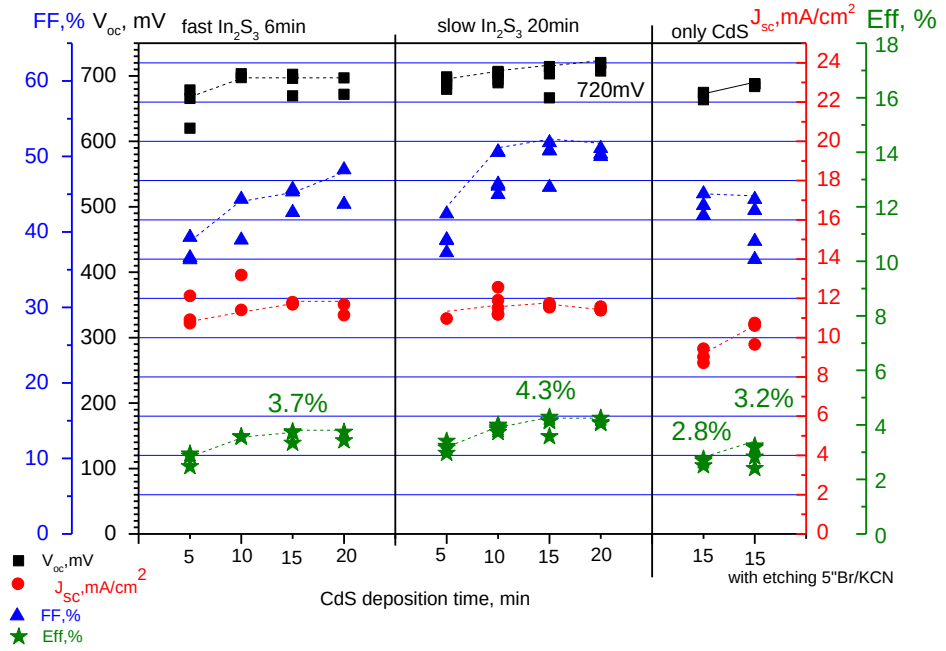

Figure 26. CZTS monograin membrane solar cell characteristic versus different CdS deposition time when In_2S_3 deposition is kept constant.

For the recipe 1 (without citric acid), the V_{oc} had an enhancement by increasing the CdS deposition time from 5-10 min and then the V_{oc} value stayed stable. The J_{sc} didn't have a big change. The *FF* increased when the CdS deposition time increased. The highest efficiency was about 3.7% with 15 min CdS deposition. For the recipe 2 (with citric acid), the V_{oc} and *FF* was boosted by increasing CdS deposition time from 5 min. and then stayed stable after 10 min. The highest efficiency was about 4.3% when CdS deposition time was 15min. Comparing indium sulphide deposition recipe 1 (without citric acid) with recipe 2, it seems that the efficiency of solar cells is higher when used recipe 2 (with citric acid) for In_2S_3 deposition in the same conditions. In conclusion, 15 min CdS deposition time is the optimal condition for the hybrid buffer layer applied onto CZTS based solar cells

4.5. Study of influence of annealing treatment after hybrid buffer layer deposition

The CZTS membranes were etched with freshly made 1% Br_2-MeOH solution for 5 seconds followed by 10% KCN solution for 5 seconds. Then deposited CdS onto membranes for 15 min used $Cd(NO_3)_2$ as Cd^{2+} source. The In_2S_3 layer was deposited onto the CdS/CZTS film for 20 min used recipe 3(added citric acid). The membranes were then subject to an annealing

varied different annealing temperature (120-160 °C) for 10 min and different annealing time (10-60 min) at 130 °C.

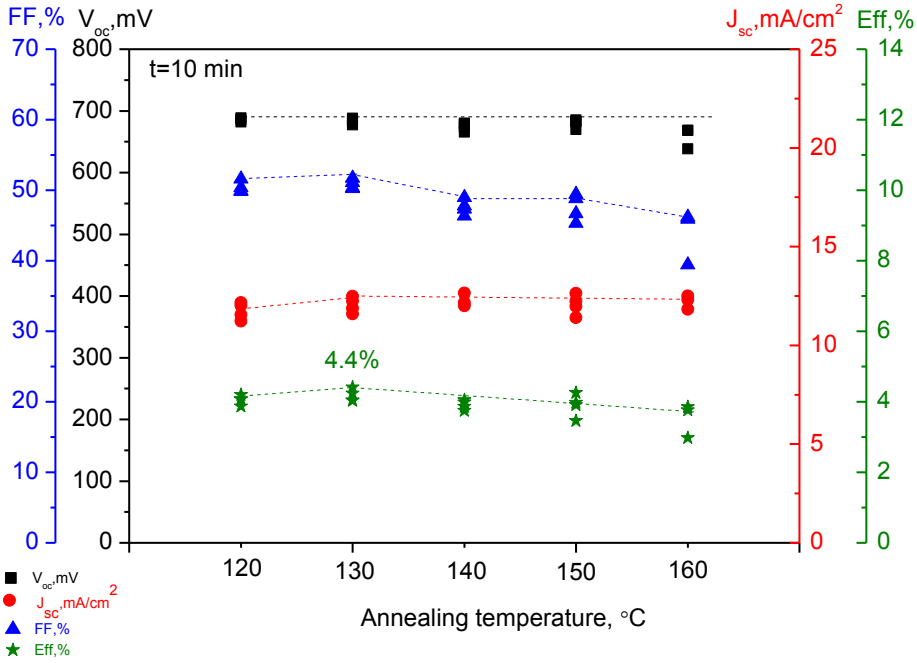

Figure 27. CZTS monograin membrane solar cell characteristic versus different annealing temperature for 10 min.

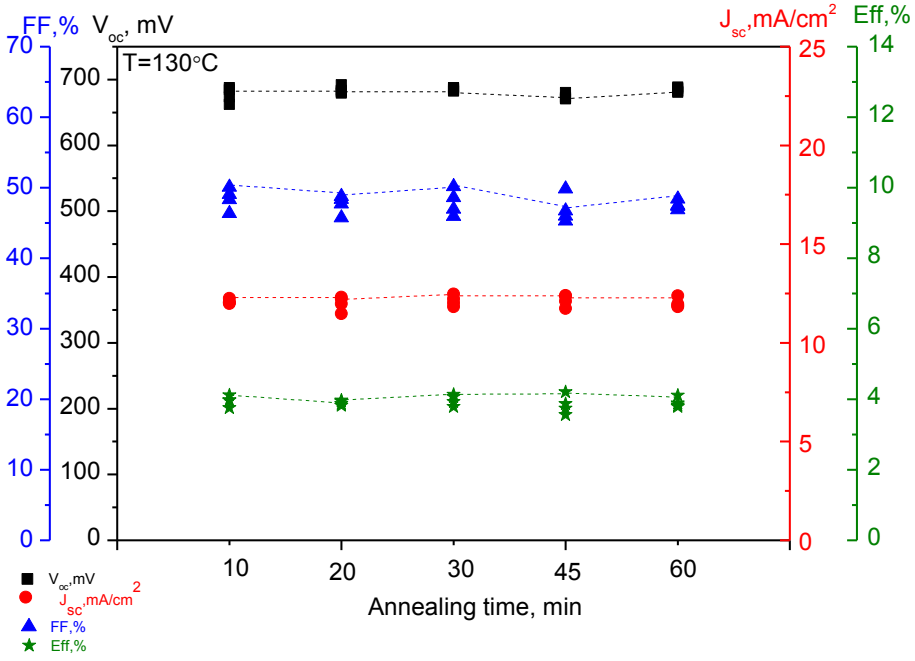

Figure 28. CZTS monograin membrane solar cell characteristic versus different annealing time at 130 °C.

Figure 27, shows the influence of different annealing temperature on CZTS solar cells. It could be seen that 130 °C is an optimal annealing temperature for CZTS solar cells. The highest efficiency achieved at 4.4% when the annealing temperature is 130 °C. When increased the temperature from 140-160 °C, the V_{oc} and *FF* had a little bit decrease. Figure 28, shows the influence of different annealing time on CZTS solar cells. It clearly seen that increased annealing time at 130 °C constant temperature, the solar cells parameter didn't change a lot and it just keep stable. In conclusion, changed annealing time didn't show a positive effect on solar cells performance.

CONCLUSIONS

The aim of this thesis was to study the possibilities to improve the CZTS-based solar cells performance by modifying the buffer layer deposition process: 1) the Cd^{2+} source and CdS deposition time and 2) by applying CdS/In_2S_3 hybrid buffer layer into CZTS solar cells.

It was found that:

1. By changing Cd^{2+} source for CdS deposition in the used CdS deposition recipe there was no big influence on CZTS solar cells performance. The highest solar cell performance and the smallest deviation of parameters have the solar cell with CdS from cadmium nitrate. .

2. Optimum CdS deposition time was found to be 10-15 minutes. Longer deposition times up to 40 minutes had no big influence on CZTS/CdS MGL solar cells performance.

3. In_2S_3 buffer layers deposited by the used recipes blocked the working ability of the In_2S_3/CZTSMGL solar cells.

4. Applying CdS/In_2S_3 hybrid buffer layer on CZTS-based MGL solar cells could improve the efficiency of solar cells in comparision with a CdS single layer. The thickness of In_2S_3 buffer layer on CdS layer has a big influence on solar cells performance. For recipe 1 (without citric acid), the optimal In_2S_3 deposition time was found to be 5 min, for recipe 2 (with citric acid), 20 min is optimal for In_2S_3 deposition.

5. As for annealing treatment, 130 °C is optimal temperature for solar cell cells performance. But changed the annealing time from 10-60 min at 130 °C did not show any obvious effect on CZTS solar cells characteristics.

ABSTRACT

In CZTS solar cells, one key issue limiting the performance is large open circuit voltage deficit, likely resulting from a non-optimal conduction band alignment between the *p-type* CZTS absorber and the *n-type* buffer layer. Therefore the aim of this work was to find out the optimum condition for deposition buffer layer for CZTS MGL solar cells to improve the solar cells parameters. The research content mainly includes three parts.

In the first part by modification of Cd^{2+} source (CdI_2, $CdCl_2$, $CdSO_4$, $CdAc_2$, $Cd(NO_3)_2$, $InCl_3$+$CdSO_4$) and deposition time (5-40 min) the optimal condition for CdS deposition were find out. In this thesis the optimal conditions for CdS chemical deposition were found as follows: deposition time 10-15 min at 45 °C if $Cd(NO_3)_2$ as Cd^{2+} source is used.

In the second part of thesis the influence of In_2S_3 buffer instead of CdS buffer was studied. The obtained results showed that In_2S_3/CZTS-based solar cells performance was worse than CdS/CZTS-based solar cells. The efficiency of In_2S_3/CZTS-based solar cells was below 1%.

In the third part the influence of In_2S_3/CdS hybrid buffer layer in CZTS MGL solar cells was studied. Compared to the single CdS buffer layer in CZTS solar cells, the In_2S_3/CdS hybrid buffer layers improved solar cell performance: not only yield an enhancement in V_{oc}, but also gave a small increase in *FF* and J_{sc} values, thereby increasing the efficiency from 2.7% to 4.6%. These hybrid In_2S_3/CdS buffers provide a promising way to reduce the V_{oc} deficit and further boost efficiency of CZTS solar cells.

KOKKUVÕTE

CZTS päikesepatarei töö üheks limiteerivaks faktoriks on puudujääk avatud vooluahela pinges, mis tõenäoliselt on põhjustatud mitte optimaalsest juhtivustsooni ühildumisest *p-tüüpi* CZTS absorber ja *n-tüüpi* puhverkihi vahel. Seega oli antud töö eesmärgiks leida optimaalsed puhverkihi sadestamise tingimused parandamaks CZTS monoterakiht päikespatarei väljundparameetreid. Uurimistöö koosneb peamiselt kolmest osast.

Esimeses osas leiti optimaalsed sadestamise tingimused varieerides Cd^{2+} iooni allikat (CdI_2, $CdCl_2$, $CdSO_4$, $CdAc_2$, $Cd(NO_3)_2$, $InCl_3$+$CdSO_4$) ja sadestusaega (5-40 min). Leitud optimaalsed tingimused CdS sadestamiseks vesilahusest on järgnevad: sadestusaeg 10-15 min 45°C juures, kui Cd^{2+} iooni allikana kasutada $Cd(NO_3)_2$ soola.

Töö teises osas uuriti In_2S_3 puhverkihi mõju CZTS monoterakiht päikesepatarei väljundparameetritele. Saadud tulemused näitasid päikesepatarei väikemat effektiivsust võrreldes standardse CdS puhverkihiga. Päikesepatarei effektiivsus jäi alla ühe protsendi.

Kolmandas osas uuriti In_2S_3/CdS hübriid puhverkihi mõju päikesepatarei väljundparameetritele. Võrreldes CdS puhverkihiga suurenesid päikesepatarei V_{oc}, J_{sc} ja *FF* tõstes effektiivsuse väärtust 2.7%-lt 4.6%-le.

REFERENCES

1. International Energy Agency, 2011. World Energy Outlook. (http://www.worldenergyoutlook.org/weo2011/)

2. Greenpeace and the European Photovoltaic Industry Association, Solar Generation VI (2011) (http://www.greenpeace.org/international/Global/international/publications/climate/2011/Final%20SolarGeneration%20VI%20full%20report%20lr.pdf)

3. International Energy Agency, 2014. Technology Roadmap, Solar photovoltaic energy. (https://www.iea.org/publications/freepublications/publication/TechnologyRoadmapSolarPhotovoltaicEnergy_2014edition.pdf).

4. William Shockley and Hans J. Queisser, "Detailed Balance Limit of Efficiency of p-n Junction Solar Cells", *Journal of Applied Physics*, Volume 32, pp. 510-519 (1961).

5. Delbos S. Kësterite thin films for photovoltaics: a review [J]. *EPJ Photovoltaics*, 2012, 3: 35004.

6. Wang W, Winkler M T, Gunawan O, et al. Device characteristics of CZTSSe thin-film solar cells with 12.6% efficiency [J]. *Advanced Energy Materials*, 2014, 4.

7. R. Haight, A. Barkhouse, O. Gunawan, B. Shin, M. Copel, M. Hopstaken, and D. B. Mitzi, Band alignment at the $Cu_2ZnSn(S_xSe_{1-x})_4$/CdS interface, *Applied Physics Letters* 98, 253502 (2011).

8. http://www.greenpeace.org/international/Global/international/publications/climate/2011/Final%20SolarGeneration%20VI%20full%20report%20lr.pdf

9. Thomas L. Floyd, "*ElectronicDevices: Conventional Current Version* ", eighth edition, Pearson International Edition, 2008.

10. Robert L. Boylestad, and Louis Nashelsky, "*Electronic Devices and Circuit Theory*", Nineth edition, Prentice Hall, 2008.

11. Green M A. Solar cells: operating principles, technology, and system applications [J]. 1982.

12. E. Mellikov, M. Altosaar, J. Raudoja, K. Timmo, O. Volobujeva, M. Kauk, J. Krustok, T. Varema, M. Grossberg, M. Danilson, K. Muska, K. Ernits, Lebnet, D. Meissner, $Cu_2(Zn_xSn_{2-1})(S_ySe_{x-1})_4$ MONOGRAIN MATERIALS FOR PHOTOVOLTAIC; *Journal of Materials Challenges in Alternative and Renewable Energy*, 2011.

13. https://books.google.com.hk/books?id=8IqQCgAAQBAJ&pg=PA34&lpg=PA34&dq=monograin+czts&source=bl&ots=Ad23tSNiS1&sig=GtT_9eBZlmSuQV1bQ3HHkIfCEeI&hl=zh-CN&sa=X&ved=0ahUKEwjn_IObx4DNAhUM6xQKHTjPCf0Q6AEISzAG#v=onepage&q=monograin%20czts&f=false

14. Altosaar M, Raudoja J, Timmo K, et al. $Cu_2Zn_{1-x}CdxSn(Se_{1-y}S_y)_4$ solid solutions as absorber materials for solar cells [J]. *physica status solidi* (a), 2008, 205(1): 167-170.

15. Kentaro ITO "Copper Zinc Tin Sulfide-Based Thin Film Solar Cells", Shinshu University, Nagano, Japan, page 290-291.

16. Hall, S.R., J.T. Szymanski, J.M. Stewart, 1978. *Can. Mineral*, 16: 131.

17. Delbos, S., 2012. *EPJ Photovoltaics*, 3: 35004.

18. Katagiri H, Jimbo K, Maw W S, et al. Development of CZTS-based thin film solar cells [J]. *Thin Solid Films*, 2009, 517(7): 2455-2460.

19. McCandless BE, Hegedus SS. *Proc. of the 22th IEEE Photovoltaic Specialists Conference*, (1991) 967–972.

20. A. Niemegeers, M. Burgelman and A. De Vos, *Appl. Phys. Lett*. **67** (1995) 843.

21. I. Konovalov and R. Szargan. *Appl. Phys. Lett*. **82** (2003) 2088.

22. R. Klenk, *Thin Solid Films* **387** (2001) 135.

23. P. Roy, and S. K. Srivastava *Mater.Chem.Phys*., 2006, 95 235–241.

24. Y.Y. Ma,andR.H. Bube, *J.Electrochem.Soc*.,1997, 124, 1430.

25. P.C. Pande, G.J. Russell, and J. Woods, *Thin Solid Films*, 1984, 121, 85.

26. A. Bayer, D. S. Boyle, M. R. Heinrich, P. O. Brien, D. J. Otway, and O. Robbe, *Green Chem.,* 2000, 2, 79.

27. Zhihua. G, Jingbing. L, Hao. W. Investigation on growth of In_2S_3 thin films by chemical bath deposition. *Materials science in semiconductor processing* 2012; 15:187-93.

28. K, Ernits, Study of In_2S_3 and ZnS Thin Films Deposited by Ultrasonic Spray Pyrolysis and Chemical Deposition. Doctoral thesis, Tallinn, TUT (2009).

29. Lokhande C D, Ennaoui A, Patil P S, et al. Chemical bath deposition of indium sulphide thin films: preparation and characterization [J]. *Thin Solid Films*, 1999, 340(1): 18-23.

30. Laurencic C, Arzel L, Couzinié-Devy F, Barreau N. Investigation of Cu(In,Ga)Se_2/In_2S_3 diffuse interface by Raman scattering. *Thin Solid Films* 2011; 519:7553-5.

31. G. Kitaev, A. Uritskaya, and S. Mokrushin, Russ. *J. Phys. Chem*. 39, 1101 (1965).

32. Hodes G. Chemical solution deposition of semiconductor films [M]. CRC press, 2002.

34. T. P. Niesen and M. R. De Guire, J. Electroceramics 6, 169 (2001).

35. L. Sillén and A. Martell, Stability Constants of Metal-Ion Complexes, Burlington House, London (1964).

36. Mane R S, Lokhande C D. Chemical deposition method for metal chalcogenide thin films [J]. *Materials Chemistry and Physics*, 2000, 65(1): 1-31.

37. Hodes G. Chemical solution deposition of semiconductor films [M]. CRC press, 2002.

38. Semiconductor Heterstructures,
https://courses.cit.cornell.edu/ece533/Lectures/handout2.pdf

39. Giorgio Margaritondo, "Electronic structure of semiconductor heterojunction", 1998.

40. Andrade-Arvizu J A, Courel-Piedrahita M, Vigil-Galán O. SnS-based thin film solar cells: perspectives over the last 25 years [J]. *Journal of Materials Science: Materials in Electronics*, 2015, 26(7): 4541-4556.

41. Minemoto T, Matsui T, Takakura H, et al. Theoretical analysis of the effect of conduction band offset of window/CIS layers on performance of CIS solar cells using device simulation [J]. *Solar Energy Materials and Solar Cells*, 2001, 67(1): 83-88.

42. Yan C, Liu F, Song N, et al. Band alignments of different buffer layers (CdS, Zn (O, S), and In_2S_3) on Cu_2ZnSnS_4 [J]. *Applied Physics Letters*, 2014, 104(17): 173901.

43. Yan C, Liu F, Sun K, et al. Boosting the efficiency of pure sulfide CZTS solar cells using the In/Cd-based hybrid buffers [J]. *Solar Energy Materials and Solar Cells*, 2016, 144: 700.

44. Kim J, Hiroi H, Todorov T K, et al. High efficiency $Cu_2ZnSn(S, Se)_4$ solar cells by applying a double In_2S_3/CdS emitter [J]. *Advanced Materials*, 2014, 26(44): 7427-7431.

45. Hiroi H, Kim J H, Kuwahara M, et al. Over 12% efficiency $Cu_2ZnSn(Se, S)_4$ solar cell via hybrid buffer layer [C]//Photovoltaic Specialist Conference (PVSC), 2014 IEEE 40th. IEEE, 2014: 0030-0032.

46. Hiroi H, Sakai N, Kato T, et al. High voltage Cu_2ZnSnS_4 submodules by hybrid buffer layer [C]//Photovoltaic Specialists Conference (PVSC), 2013 IEEE 39th. IEEE, 2013: 0863-0866.

47. M. Altosaar, T. Varema and E. Mellikov, Surface degreasing and activation as important factors for Cu Electroplating on ITO substrates, International DAAAM Proceedings, 22-29th April, 2000, Tallinn Estonia, pp. 233-235.

48. M. Kauk-Kuusik, K. Timmo, M. Danilson, M. Altosaar, M. Grossberg, K. Ernits, *p–n* junction improvements of Cu_2ZnSnS_4/CdS monograin layer solar cells. *Applied Surface Science* 357 (2015) 795–798.

49. Timmo K, Altosaar M, Raudoja J, et al. Chemical etching of $Cu_2ZnS(SSe)_4$ monograin powder [C]// Photovoltaic Specialists Conference (PVSC), 2010 35th IEEE. IEEE, 2010: 001982-001985.

50. Fairbrother A, García-Hemme E, Izquierdo-Roca V, et al. Development of a selective chemical etching to improve the conversion efficiency of Zn-rich Cu_2ZnSnS_4 solar cells [J]. *Journal of the American Chemical Society*, 2012, 134(19): 8018-8021.

51. Gao Z, Liu J, Wang H. Investigation on growth of In_2S_3 thin films by chemical bath deposition [J]. *Materials Science in Semiconductor Processing*, 2012, 15 (2): 187-193.

52. Gopinath G R, Miles R W, Reddy K T R. Influence of Bath Temperature on the Properties of In_2S_3 Films Grown by Chemical Bath Deposition [J]. *Energy Procedia*, 2013, 34: 399-406.

53. P.S.Priambodo, N.R. Poespawati, D. Hartanto, "Chapter book: Solar Cell Technology", INTECH Open Access Publisher, ISBN 978-953-307-316-3, www.intechweb.org.

54. M.A. Green, "Solar Cells, Operating Principles, Technology and System Applications," Prentice Hall, ISBN 0-13-82270, 1982.

55. Jiang F, Harada T, Kuang Y, et al. Pt/In_2S_3/CdS/Cu_2ZnSnS_4 Thin Film as an Efficient and Stable Photocathode for Water Reduction under Sunlight Radiation [J]. *Journal of the American Chemical Society*, 2015, 137(42): 13691-13697.

ACKNOLEDGEMENTS

This thesis is based on the experimental work carried out at the Department of Material Science, Tallinn University of Technology.

First, I would like to thank my supervisor, leading research scientist Mare.Altosaar, for her excellent guidance, continuous support and fruitful discussions during my research work.

I would like to thank the members of the research group who have contributed to my thesis: Maris Pilvet (co-supervisor), Marit Kauk-Kuusik, Kristi Timmo, Jaan Raudoja, Tiit Varema, Valdek Mikli for their continuous help and support.

I would like to thank PhD Tiit Varema who agreed to review this master thesis.

Last, I want to thank my family members and friends for their support that helped me to finish my thesis.